Bladed Disks: Non-Linear Dynamics

J. SZWEDOWICZ
Switzerland

1.0 INTRODUCTION

To prevent turbine axial blades from HCF failures, caused either by harmonic or by non-engine excitation like flutter or severe part load conditions, a freestanding airfoil can be coupled circumferentially in different manners. Blades with integrally machined shrouds or winglets, lacing wires or zigzag pins, which are threaded through a hole in the airfoil, are used often for minimizing the resonance responses. The bladed disc vibrations are characterized with the well-known interference (or the nodal diameter) curves and Campbell diagrams (see e.g. Ewins, 1973), while non-linear blade vibrations are assessed usually by using the performance diagram (Griffin and Labelle, 1996). Besides the friction dissipation on a shroud, a winglet or on a wire contact, friction dampers are in widespread use in disc assemblies with freestanding blades to control their vibration amplitudes. Several designs, such as a dog bone, a pin type or a wedge damper are employed in turbine blade design as devices for the frictional damping. In a comprehensive manner Srinivasan (1997) outlines different aspects of the linear and non-linear dynamics of the tuned and mistuned disc assemblies, and there can be found more details.

The non-linear dynamics of rotating blades corresponds principally to the physical phenomena of

- Friction dissipation (see Figure 9-1a)
- Elastic impacts or (Figure 9-1c)

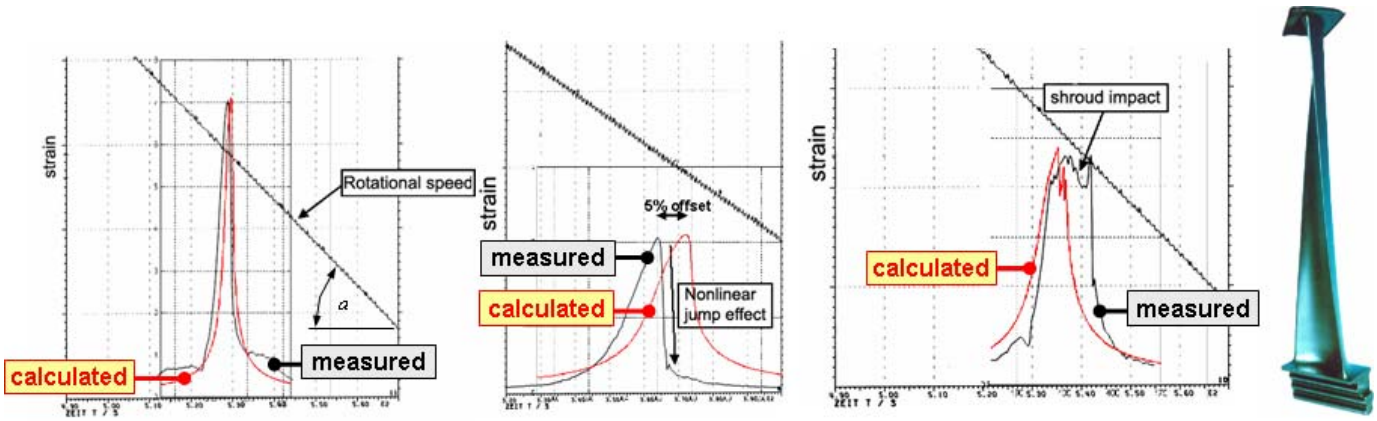

a) b) c)

Figure 9-1: The measured (black lines) and computed (red curves) resonance response functions (RRF) of the shrouded blade passing its resonances in the spin pin condition and excited by an air jet (Szwedowicz et al., 2003).

a) Example of the RRF damped by the friction dissipation at the shroud contact

b) Case of the RRF with a rapid jump on the shroud interface caused usually by non-linearities on the contact

c) Instance of the RRF with chattering of sliding contacts of the shroud coupling

Both of them as chattering (impacts) of sliding contacts of the airfoil interfaces (Figure 9-1c).

At the blade root, only micro-sliding can occur due to the high centrifugal forces acting on the root contacts. At the shroud or winglet coupling, chattering of sliding contacts can occur, since the resulting normal contact force would be smaller than resonance reaction forces induced by the excitation load acting on the rotating blade. From the engineering point of view, impacts are undesired physical circumstance, which could lead towards fretting problem (Szwedowicz et al., 2005). In practice, the phenomena of impacts are seldom used for suppressing of resonance stresses of rotating blades, because of some technical difficulties in realization of those types of the dampers. Quite contrary to that, friction dampers are much more straightforward in their real application. Therefore, the non-linear dynamics caused by impacts of sliding contacts will be not taken into account in this work. In case of interest, theoretical backgrounds for the impact damper application in the rotating blade can be found in Duffy's work (2000), which provides also the experimental verification.

In general, alternating stresses among other things depends on the overall damping properties, which are caused by friction, aerodynamic viscous and hysteresis dissipation in material. These three damping sources in rotating turbine blades are shortly discussed here in relation to the well-defined practices used in engineering analyses. Following the historical development of a friction damper, showing typical damper's examples and explaining the fundamental theoretical backgrounds of the Harmonic Balance Method used for the linearization of friction forces, the physical interpretation of blade vibrations with friction dissipation at shrouds and on under-platform dampers is mainly taken into consideration. Aspects of contact stiffness, calculations of contact forces, uncertainty margins of friction coefficients and excitation levels is brought together with respect to needs for the design process.

2.0 THEORETICAL BACKGROUNDS OF FORCED VIBRATIONS WITH FRICTION

For many years the friction damping capability has been developed for rotating disc assemblies. At the beginning this process is based mainly on very simple analytical analyses and empirical knowledge. The understanding of the friction dissipation was gathered from various measurements on special test rigs, and from the experiences of the operating blade with friction devices. For the last 10 years, the numerical prediction of forced vibrations of the rotating blades with friction damping has done a remarkable progress. The existing numerical tools can predict the vibration blade with friction in more reliable manner. However, the experimental validation of these results seems still to be required. General difficulties in the mathematical description of the contact dynamics is the local elastic contact deformations, micro-slips deformations on sliding contacts as well as the variable normal contact forces, as it is illustrated in Figure 9-2a. In practice, an additional problem is to determine wear rate of sliding contacts (see Figure 9-2b), which also involves experimental verification.

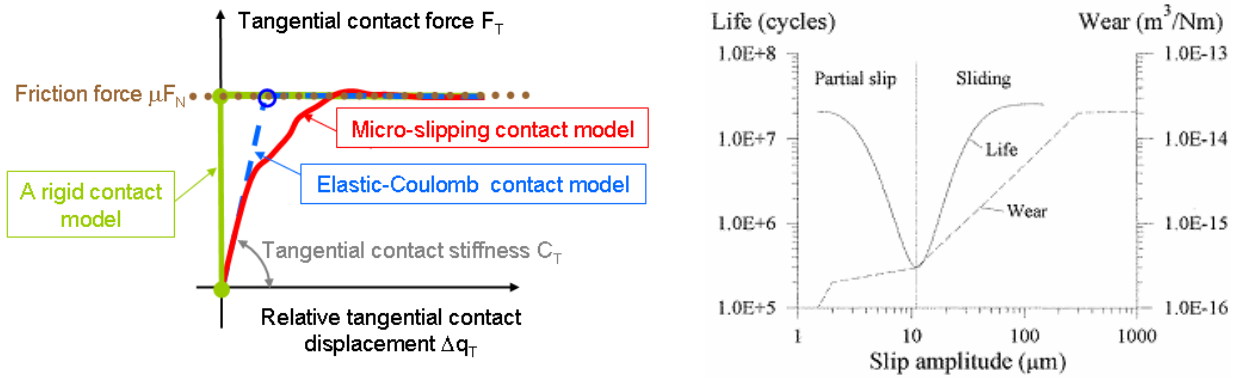

a) b)

Figure 9-2: a) Typical relationships between slip amplitude, tangential contact stiffness C_T and normal contact load F_N, where μ denotes static friction coefficient, b) Relationships among slip amplitude, wear rate, and fretting life (Vingsbo and Söderberg, 1988).

According to Vingsbo and Söderberg's (1988) investigation, relative micro-slips on the contact should be below *2 μm* to suppress the wear of contacting parts. This is schematically demonstrated in Figure 9-2b. Indeed, these relationships among slip amplitude, wear rate, and fretting life need to be known for the material pair of interest for different temperatures. The required small micro-slips, as shown in Figure 9-2b, can be obtained technically by applying high normal contact stresses. However, too high contact stresses on the shroud interface may induce a creep problem at elevated operation temperature. The creep deflection at the airfoil tip can lead towards loosing the contact between the shrouds (DiCristoforo and Elledge, 2004). From a practical point of view, in spite of the allowed micro-slip amplitude of *2 μm*, which may be difficult to attain for the real shrouded blade, more feasible criteria need to be provided for reliable static and dynamic shroud coupling. The useful methodology, applied to the redesign of the shroud coupling due to its fretting, is presented by Szwedowicz et al. (2005). This numerical straightforward concept is based on the finite element static and free vibration computations, which are used in non-linear simulations of the shrouded blade vibrations with friction dissipation. To understand well this kind of the analysis, it is necessary to overview a development of solution manners applied to blade vibrations with friction damping, which is given in the open literature.

Probably the first analytical analysis of forced vibrations with friction dissipation was performed by den Hartog in 1931. He considered a spring-mass system with the neglected viscous damping *d*. By using his equivalent viscous damping force, which approximates friction Coulomb force F_μ, (Figure 9-3a) as

$$1) \quad F_\mu \cong \frac{4}{\pi} \mu_d \, F_N \, ,$$

the solution of the forced vibration of one degree of freedom (1dof) system (see Figure 9-3b)

$$2) \quad m\ddot{u} + d\dot{u} + ku = F_o \cos(wt) - F_\mu$$

provides the satisfied results for large displacements. In equation (1) μ_d denotes the dynamic (called also sliding or kinetic) friction coefficient and F_N is the normal contact force (see Figure 9-3b). Nevertheless, a non-linear nature of the friction Coulomb force on a rigid contact has to be described by

$$3) \quad F_\mu = \mu_d \, F_N \, sgn(\Delta\dot{u}) = \mu_d \, F_N \frac{\Delta\dot{u}}{|\Delta\dot{u}|},$$

where $\Delta\dot{u} = \dot{u}_1 - \dot{u}_2$ means the relative velocity of oscillating contacts of body *1* and *2* ($\dot{u}_2$ equals *0* in Figure 9-3). According to equation (3), the relationship between the friction Coulomb force, relative velocity $\Delta\dot{u}$ and relative deformation Δu of oscillating contacts is shown in Figure 9-3. The friction force is a periodicity function in the time domain *t*. Then, by applying the Fourier transformation, the non-linear periodical friction force F_μ with its vibration period $T=1/\omega$ can be represented as a sum of linear harmonic functions, what is expressed by

$$4) \quad F_\mu = \frac{4}{\pi} \mu_d \, F_N \sum_{k=1,3,\ldots,}^{\infty} \frac{(-1)^k}{k} \left(cos(k\omega t - \beta_k)\right),$$

where *k* denotes the *k*-th Fourier harmonic, β_k means the phase delay of the friction force F_μ with respect to the excitation force $F(t)=F_o cos(\omega t)$ for excitation frequency ω *(rad/s)*. By substituting equation (4) into (1), and considering the harmonic response as

$$5) \quad u(t) = \sum_{k=1,2,3}^{\infty} u_k \left(cos(k\omega t - \gamma_k)\right),$$

the forced vibration of the 1dof system can be solved by using the harmonic balance method (HBM). It means that the unknown response amplitudes u_k and its phase delays γ_k in equation (5) are equated individually to zero for each harmonic *k*.

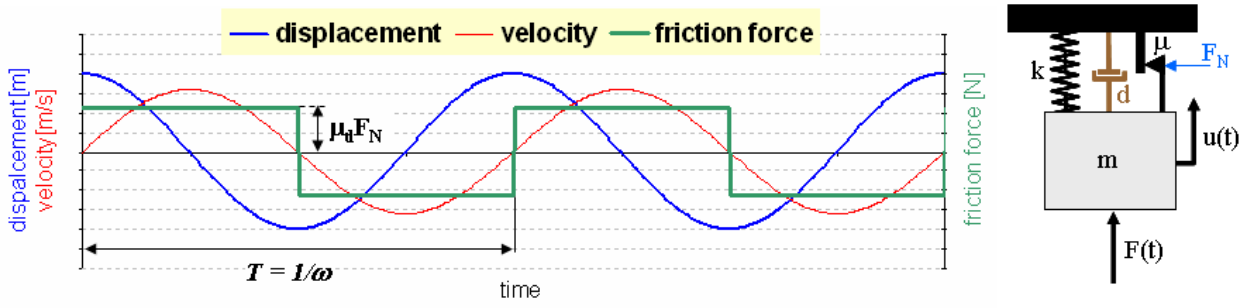

a) b)

Figure 9-3: a) Relationship between the vibration and Coulomb friction force for harmonic excitation *F(t)* with vibration period *T=1/ω*, b) One degree of freedom system with a rigid contact model, where *m*, *d*, *k*, and μ are mass, viscous damping, stiffness, and friction coefficient (see equation (1)), respectively.

The den Hartog's formulation (1956) was developed further by different researchers and at the beginning applied mainly to riveted and bolted joints in airframe systems (Earles, 1996, Mott, 1970, Earles and Mott, 1972). First theoretical investigations of blade vibrations with friction dampers appeared in the 70s. The major

motivation of these works was current design practice, which allowed for adding additional lacing wires or zigzag bolts into the turbine stage in circumstances of not sufficient aerodynamic and material damping for reducing resonant amplitudes to the acceptable level. Earles and Williams (1972, 1974) extended den Hartog's formulation by developing a new linearization concept of the non-linear friction force on a rigid contact. Their approach provides closed-forms for the general response of the system for slipping and sticking contact conditions at the damper interface. Earles and Williams' numerical results are found in good agreement with the measurements done at the non-rotating set-up with *2* parallel-sided cantilever beams like freestanding blades. The similar models of single contact point representing the whole contact coupling and oscillating in one-direction on a rigid interface were applied by different researchers, like Muszynska and Jones (1978, 1983) for modeling of tuned and mistuned disc assemblies.

Already the measurement of den Hartog's (1931) has demonstrated the hysteresis relationship between the tangential force and tangential displacement on the contact. This hysteresis, illustrated in Figure 9-4, is caused by local elastic deformations between contacting bodies and it is modeled usually by the resulting elastic stiffness C_T for the sticking contact condition. This nonlinear friction damper behavior can be defined by the equivalent complex stiffness, which depends on the response amplitude of the system. The dynamic equation is then solved in the modal domain using the harmonic balance method regarding a one-term or multi-term Fourier harmonics *k*. The reliability of the numerical solution increases by applying more harmonics *k* in the linearization of the nonlinear friction force (Wang and Chen, 1992). This corresponds to more accurate representation of a hysteresis loop (see Figure 9-5b).

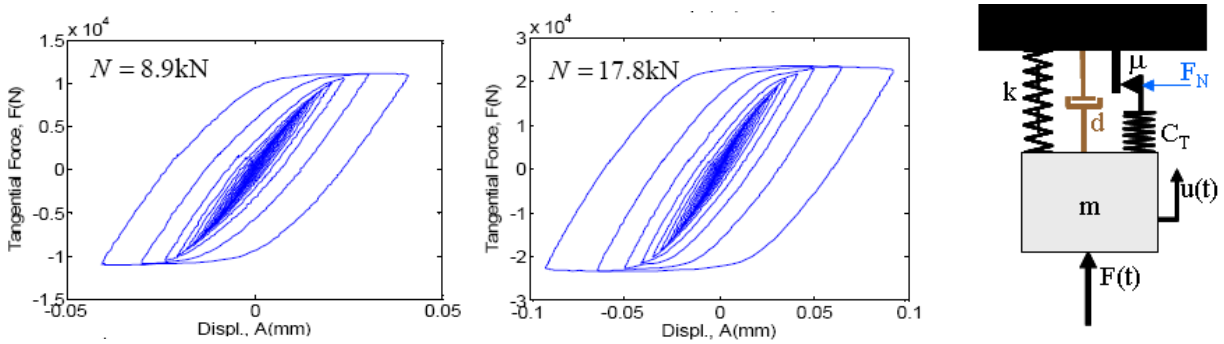

a) b)

Figure 9-4: Experimental hysteresis curves measured with quasi-static tests by Koh et al. (2004), where *N* denotes the normal contact force and *A* is the tangential displacement, which can be mathematically represented by the macro-slip or the micro-slip contact approach, b) One-degree-freedom system with macro-slip contact approach for the constant tangential contact stiffness (C_T = *const*).

In Figure 9-5, the well-known models for the approximation of a hystersis frictional loop are presented. In 1980, Griffin applied the macro-slip approach (Figure 9-5b) to optimization of the resonance responses of the lowest mode shape of the high pressure turbine blade with a frictional damper. The damper was mounted under a platform of the airfoil. Considering the contact between the cylindrical damper interface and a flat contact of the under-platform of the airfoil, his experimental data confirmed well the numerical results, which were based on the macro-slip approach. Griffin has identified that the tangential contact stiffness C_T between the damper and blade interface is a crucial parameter in the damper optimization.

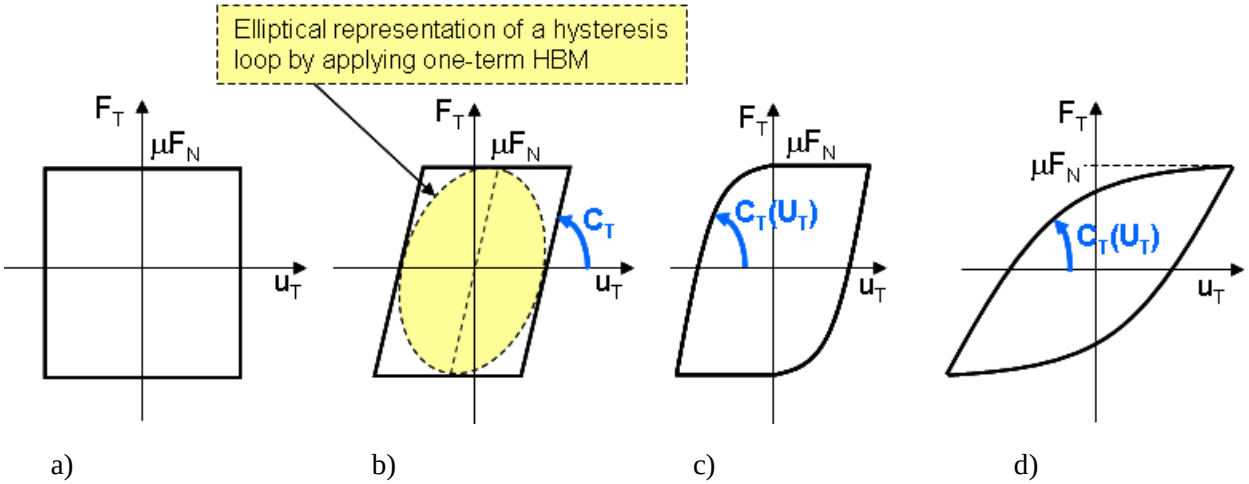

Figure 9-5: Theoretical models of a hystersis loop describing the elastic contact behavior with friction a) Coulomb frictional damping loop (a rigid contact model, see *1dof* system in Figure 9-3b for the tangential contact stiffness $C_T = \infty$), b) macro-slip frictional damping loop for the constant tangential contact stiffness ($C_T = const$), see *1dof* system in Figure 9-4b, c) micro-slip frictional damping loop (Cattaneo-Mindlin's model) variable contact stiffness $C_T(U_T) \neq const$, where U_T denotes the tangential response amplitude on contact, d) Exponential micro-slip frictional damping loop (Sanliturk, et al. 1999) with variable C_T.

Using Hertz's (1882) analytical formulas, the normal contact stiffness C_N can be determined from the local normal elastic deformations between two contacting bodies. For the case of zero shear contact deformation and the circular contact area, Mindlin (1949) derived analytical formulas. His method allows for the micro-slip contact condition between smooth spherical bodies regarding Coulomb's friction law. Mindlin's analytical ratio of the elastic normal contact stiffness C_N to the elastic tangential contact stiffness C_T can be expressed in the empirical form as

$$6) \quad \frac{C_T}{C_N} = \frac{4G}{E},$$

where G and E denote the shear (Kirchhoff's) and elasticity (Young's) modulus of the bodies in contact, respectively. Equation (6) was experimentally verified by Balmer (1992) and Burdekin et al. (1978). However, its reliable application is limited only to circular contact conditions. For the elliptical contact area for two non-spherical elastic bodies, Deresiewicz (1957) worked out the relationship between the normal C_N and tangential C_T contact stiffness by assuming the constant normal contact stress distribution. By considering the variable tangential contact stiffness C_T in terms of the unknown tangential response amplitude at contact u_T, the macro-slip contact approach was extended on the micro-slip contact approach, whose frictional loop is illustrated in Figure 9-5c. Based on the micro-slip contact approach and the measurements of frictional loops, Sanliturk et al. (1999) proposed the exponential loading curves (Figure 9-5d), which characterize the gradual and continuous dependency of the tangential contact stiffness on the partial slip, formulated earlier by Rogers and Boothroyd (1975).

Furthermore, the one-dimensional motion of the contact point was replaced with a model of the two-dimensional motion, which was proposed by Zimitrowicz (1981), Griffin and Menq (1991), Sanliturk and Ewins (1996) as well as Sextro et al. (1996). Sextro applied his *2D* point contact model to Hertzian contact by

considering *2* translations and one rotation degrees of freedom. An additional remarkable progress in the contact definition was a discretisation of the whole contact area with many contact points (Sextro et al., 1997, Sextro, 2000, Szwedowicz et al, 2001, 2003, 2005, Petrov, 2007, Cigeroglu et al., 2007). The contact discretisation can considerer partial micro-slip and stuck contact conditions at each point individually. The simulation with many contact points provides good agreements with the measurements as it is illustrated in Figure 9-1 for the steam shrouded blade, which was measured in the spin pit condition (vacuum). Petrov's approach (2007) with the discretisation contact and with his unique analytical formulation of the point contact conditions allows for modeling of complex elastic parts, like spatial sealing strips. His numerical results identify the contact regions with sticking, partial slip-stuck, slipping contact conditions as well as the separation in the contact.

A further progress in the numerical simulation of the elastic contact of vibrating parts is going to provide important inputs for qualitative fatigue life prediction. However, the reliability of this kind of fatigue assessment depends on some physical uncertainties like friction coefficients as well as unknown excitations acting on the rotating blades.

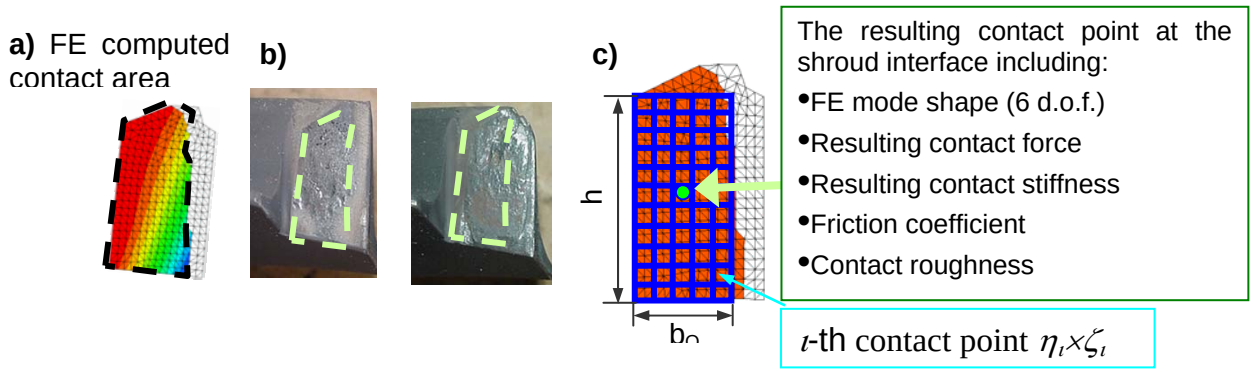

Figure 9-6: Contact of the shroud coupling (Szwedowicz et al., 2005) a) FE computed contact area, b) photos of the real contact interface with fretting damages, where dashed line corresponds to the contour of the FE contact area, c) discretisation of the FE contact area by 55 points for the non-linear dynamic analysis.

During the last 28 years, various numerical techniques have been developed for consideration of friction dissipation in the blade dynamics. These works show that the FE time-marching approach is too time consuming solution in relation to the Harmonic Balance Method. The transient FE dynamics is used sometimes for the verification the results obtained from the HBM. In general, most of these approaches employ a reduced order of the FE models and the harmonic balance method to decrease significantly the time needed for the solution of the non-linear algebraic dynamic equations including friction forces. A large number of papers on the numerical modeling of the frictional dissipation between shrouds and on under-platform friction dampers can be found in the open literature. Cameron *et al.* (1987), Griffin (1980), Wang *et al.* (1990a, 1990b, 1991, 1993), Yang and Menq (1998a), Sextro *et al.* (1997), Csaba (1999), Sanliturk *et al.* (2001), Petrov and Ewins, (2003), and Petrov (2005) provide thorough reviews of the available literature and methods solving non-linear vibrations of mechanical systems with friction. Petrov's interface element (2003, 2005, 2007) describes analytically the non-linear contact behavior at specified contact point. These elements minimize the computational effort required for the analysis of the non-linear damper-blade dynamics approximated with more complex Fourier coefficients. His method allows efficient modeling of mistuning effects caused by manufacturing tolerances of blades as well as by variation in damper contacts within a

blade-disc assembly (Petrov and Ewins, 2003). A mistuned disc assembly is modeled using mode shapes from a cyclic symmetric FE model of the tuned blade assembly as input (Feiner and Griffin, 2002, Petrov, 2004). Other approaches for the dynamic analysis of the mistuned blades including the variation in damper configuration are based on a sensitivity analysis and the assumption of a Weibull distribution. This procedure is validated experimentally and numerically with Monte-Carlo simulations as it can be found in Goetting *et al.*, (2001, 2004).

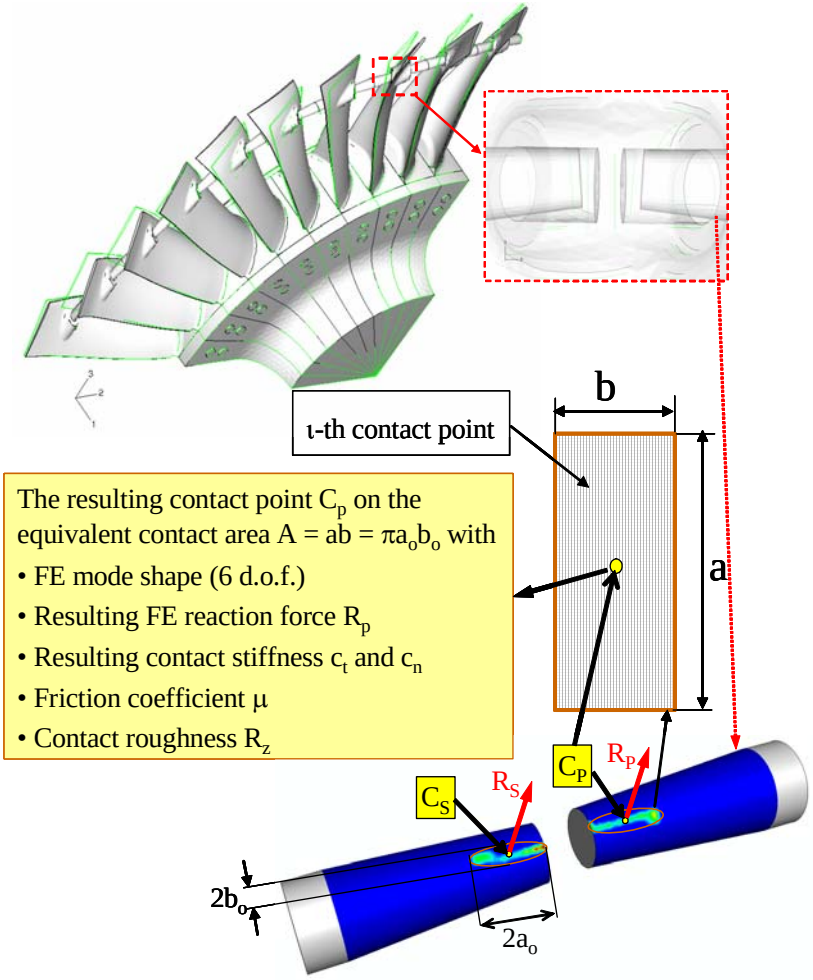

Figure 9-7: Discretesiation of the real elliptical contact area of the frictional bolt in the simplified rectangular form for the non-linear blade dynamic analysis including frictional micro-slips (Szwedowicz et al., 2008).

The remarkable and permanent progress in the theoretical modeling and in the utilization of the friction dampers started from Griffin's paper in 1980 as it is schematically illustrated in Figure 9-8. Since that time, general interest in the friction damper technology has been shown by different manufacturers of aero-engines and industrial turbines. These companies have been collaborating with various universities. Their work is usually arranged in various research programs, such as:

- FVV, Forschungsverienigung Verbrennungskraftmaschinen in Germany (e.g. Goetting, 2001)

- The GUIde Consortium: Government, Universities, and Industry Working Together to Develop New Technologies in USA
- ADTurB research program (Aeroelastic Design of Turbine Blades) funded by the European Community

or bilateral collaborations, like

- FIAT-AVIO and Politecnico di Torino,
- SNECMA and Ecole Centrale de Lyon,
- Leibniz University in Hannover and Siemens,
- Imperial College London and Rolls-Royce.

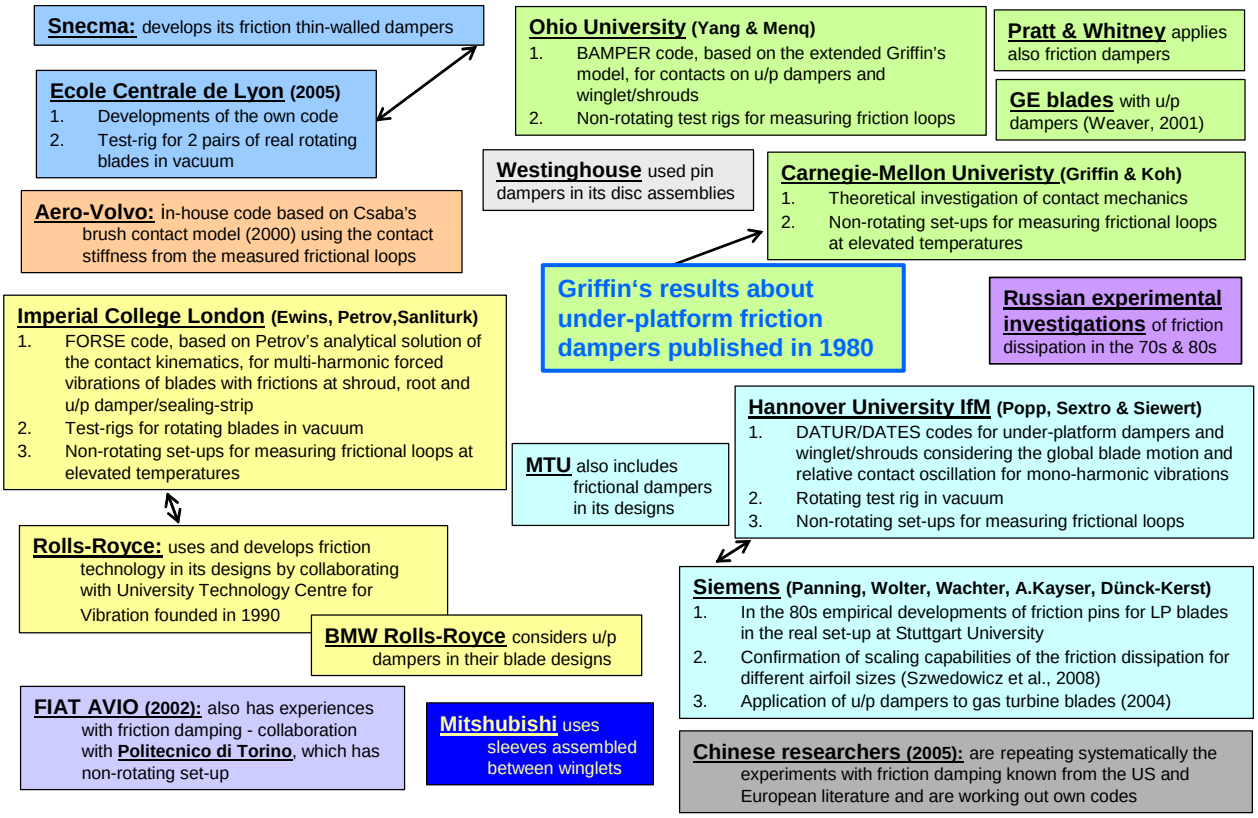

Figure 9-8: The most important R&D centers and universities working on friction damping for rotating blades and companies, which are interested in this technology.

According to the open literature, only a few R&D centers are known with their long experiences in the blade dynamics including friction, such as:

- Carnegie-Mellon Univeristy (Proff. Griffin) or Ohio University (Prof. Menq) in the USA
- and Imperial College London (Prof. Ewins, Dr. Petrov, Dr. Sanliturk), Hannover University IfM (Prof. Popp), Ecole Centrale de Lyon or Politecnico di Torino in Europe.

These universities have set-ups, which are used for the experimental assessment of the tangential contact stiffness at different temperatures. Some of them have also rotating test rigs, which allow for measurements of single disc with real blades or beams like airfoils with under-platform dampers in vacuum (e.g. Figure 9-9).

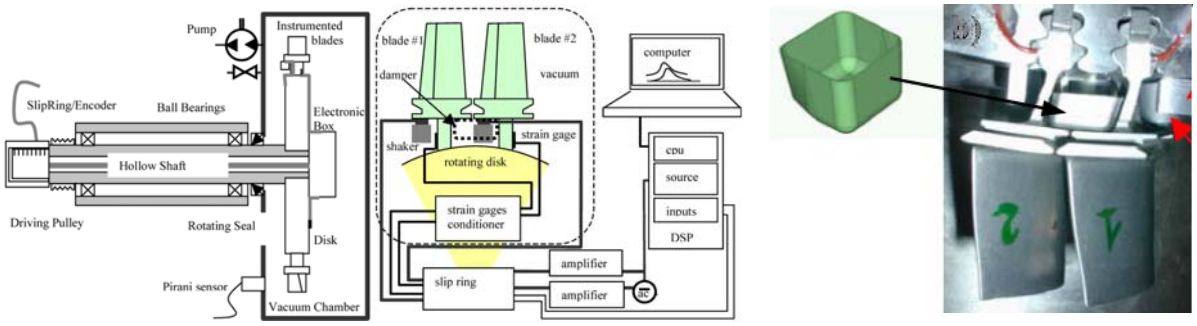

a) b)

Figure 9-9: Experimental set-up at Ecole Centrale de Lyon in France for measuring real blades with under-platform friction dampers in vacuum condition (Szwedowicz et al., 2006).

From the theoretical point of view, the contact mechanics between the shrouds (winglet) have a lot of similarities with the theory describing the non-linear dynamics of under-platform friction dampers. However, only few papers deal with the forced vibration problems of shrouded discs. Griffin and Labelle (1996) presented a practical procedure for systematic damping analysis of shrouded blades taking into account mistuning effects of the real bladed disc and magnitudes of excitation forces in the spin pit environment. By their validation of the numerical results with the experimental data, they found some general difficulties in numerical predictions of strong nonlinear behavior of the measured commercial fan blades by applying the BDAMPER code (Yang and Menq, 1997). For designers, Griffin and Labelle (1996) propose some practical issues for the effective data presentation of non-linear vibrations of the shrouded blades. They assumed a constant friction coefficient of *0.4* for the analyzed titanium shrouds and estimated magnitudes of the normal contact forces from shroud dimensions and acting centrifugal loads. Borishanskii (1974) presents experimental results of the damping capabilities of the blade with shroud. Considering one-term HBM harmonic, Sextro (2002) developed efficient solution methods for calculating the spatial forced vibration of elastic structures with friction contacts including micro-slip effects due to roughness. His approach is implemented in the HADES and DATES codes for forced vibrations of the shrouded disk assemblies with non-linear friction and impact effects. The useful numerical and experimental investigations about the dynamics of the shrouded blade are given by Szwedowicz et al. (2003, 2005 and 2008). FORSE code from Imperial College London (Petrov, 2007) provides solutions for the blades dynamics with friction, which can be taken into account on contacts of elastic 3D sealing strips, shrouds and under-platform dampers.

A very few papers consider forced vibrations problems of blades with friction bolts. The damping capability of pins within low pressure steam turbine blades numerically was investigated by Szwedowicz et al. (2008a, 2008b). The obtained numerical results correspond very well to the experimental data. In addition, the non-linear vibration results show that the damping capability of the analyzed friction pins can be scaled for different blade dimensions, since their vibrations do not experience too large response amplitudes. Indeed, the harmonic balance method allows only for vibration analyses of the system with low resonance amplitudes.

In recent years, the friction damping in blade roots is in interest of researchers. Most of the papers study experimentally those phenomena, like for instance the work of Kielb and Abhari (2003), who investigated the

high pressure turbine blade with a fire-tree root. According to the experimental investigations of Matveev et al. (1970), the dissipation at the hinged radial roots does not differ from the damping ratio measured at standstill. These experimental damping values practically are equal to the material damping ratio, unless the bending load acts on the airfoil. Under a centrifugal load of *30 kN* and a temperature of *350°C*, the measured damping ratio ξ at the radial root, made of titanium alloy, increases linearly from *0.03%* up to *0.7%* by changing the bending load from *0* up to *350 N*. At ambient temperature and no acting pressure, the measured modal damping ratio varies between *0.01%* and *0.03%* under a centrifugal force of *30 kN* (Matveev et al., 1970). These damping ratios correspond almost to the material damping of titanium alloy. These experimental investigation show that, relative frictional sliding motions between the blade root and the rotor disc are negligible because of high centrifugal stresses and in addition of pre-assembly forces within the root. The theoretical investigations of the friction damping in the root are presented by Chareleux et al. (2004), Petrov and Ewins (2004). These authors apply the similar approaches based on the laws of unilateral contact and friction, which are applied to a certain number of contact elements representing the mechanical interfaces of the blade root. These simulations permit for obtaining partial slipping as well as partial contact separation, thus the effective damping capability can be predicted in terms of rotational speed and friction coefficient.

The elaborated mathematical models for simulations of the blade dynamics with friction are sufficiently mature for performing sensitivity analyses of non-linear forced vibrations (Petrov, 2005, Panning et al., 2004, Szwedowicz et al., 2001, 2003 and 2008b). However, the reliability of these investigations depends strongly on the correct assessment of friction coefficients as well as the values of the contact stiffness. Regarding these uncertainties, this report presents the engineering methodology, based on the non-linear and the linear numerical blade dynamics with friction, for designing blade couplings, like shrouds, winglets, lacing wires, zigzag pins or under-platform dampers. Active dampers, like for instance systems using the piezoelectric technology, are not discussed in this work. In fact, active damping technologies have still some technical limits considering the range of allowable temperatures in service. This report considers only passive manner of vibration control for rotating disc assemblies.

3.0 TECHNICAL ASPECTS OF FRICTIONAL DISSIPATION USED IN ROTATING BLADED DISCS

Resonance stresses, which lead to the failure of the rotating blades, can be effectively suppressed by the friction dissipation. Figure 9-10 shows that the resonance stress of the industrial low pressure steam turbine blade is reduced *6* times by friction bolts. These bolts are loosely assembled within holes of the adjacent airfoils at standstill.

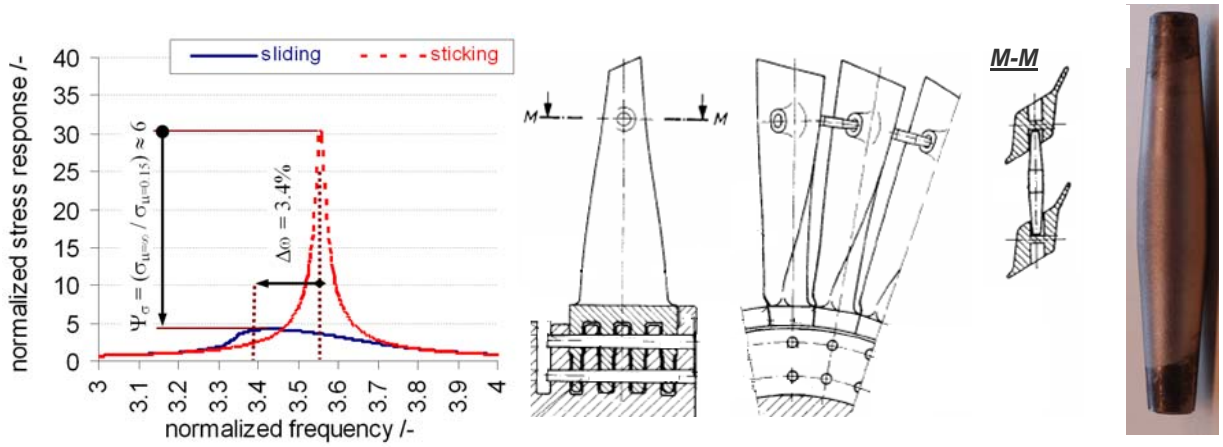

a) b)

Figure 9-10: a) Reduction of the resonance stress of the industrial low pressure turbine stage by loosely assembled frictional bolt, where "sliding" and "sticking" denote contact conditions on interfaces of the bolt (Szwedowicz et al., 2008), b) Photo of the real friction bolt after 20 years.

The technical principle of the friction dissipation in rotating blades is identical for all devices known in heavy turbines and in aero-engines, which are patented in a very large number. The friction damping can be considered either between adjacent blades on their shroud (winglet) contacts or on friction devices loosely assembled between adjacent blades. Under the operation condition, the rotating blades untwist themselves due to the centrifugal load. For the blade untwist determined at the operation condition of interest, the normal reaction forces between the shrouds (winglet) can be controlled. In case of the individual friction device, like a bolt shown in Figure 9-10, the centrifugal load pushes the friction device against the contacts of the adjacent airfoils and generates normal reaction contact forces. These contact forces depend on a mass of the friction device, its radial position and the rotational speed.

Since the fundamental natural frequency of the unrestrained (free-free boundary conditions, Figure 9-11) friction damper is significantly higher than the blade eigenfrequency of interest, the damper can be treated as a rigid device in computations. It means that its individual vibration does not participate in the blade dynamics. In other words, the motion of a rigid friction damper can be described properly with its rigid body mode shapes. This is illustrated in Figure 9-11 for the friction bolt applied to the Siemens LP steam turbine blade. The first natural frequency of the unrestrained friction bolt is *40* times higher than the first bending eigenfrequency of the freestanding LP steam turbine blade, which is considered for the friction damping. Since the eigenfrequencies of the free-free friction damper are in the range of the blade eigenfrequencies, which are considered for the friction dissipation, then the multi-harmonic balance method needs to be used in the simulation (see details in Petrov, 2007).

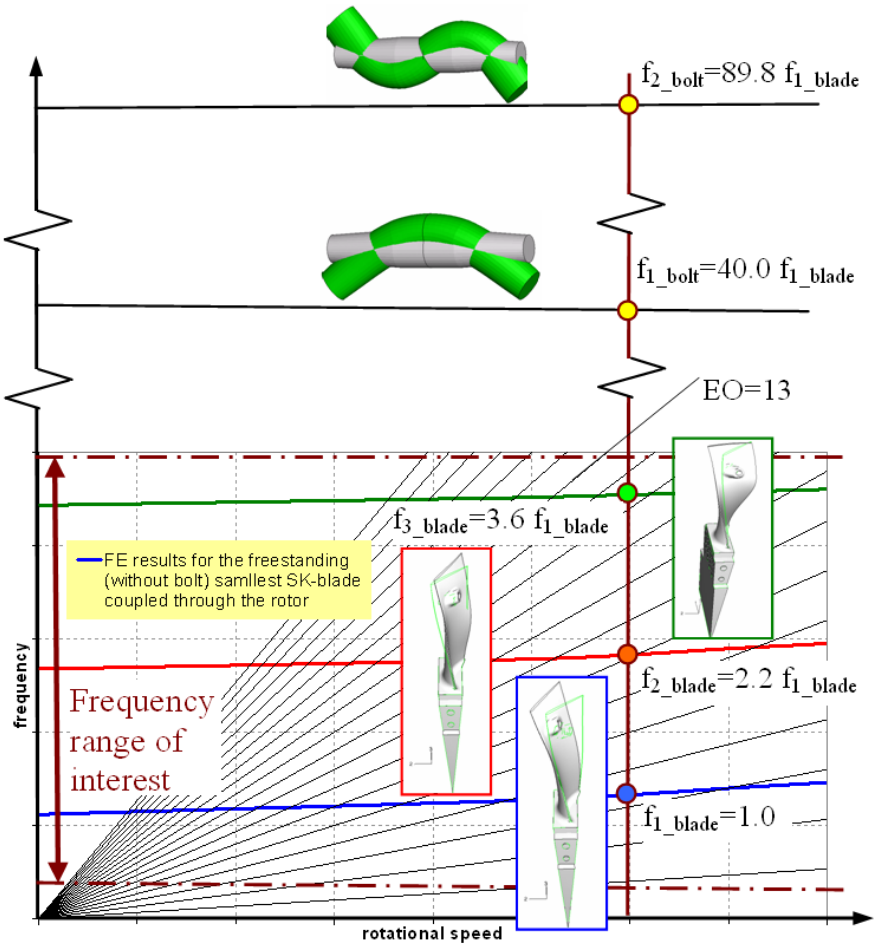

Figure 9-11: Relationship of the lowest natural frequencies of the unconstrained friction bolt to the resonance frequencies of the freestanding LP blade in the computed Campbell diagram.

The most of friction devices, which are reported in the open literature, have a solid design of very compact dimensions, which are given in various shapes. The feature of the compact damper design allows for getting high natural frequencies of the unconstrained friction damper with respect to the lowest eigenfrequencies of the freestanding blade. Some of typical compact under-platform dampers are presented in Figure 9-12. These dampers are used for the friction damping of the lowest resonance frequencies of the rotating freestanding blades. Alternatively, a thin-walled structure (Figure 9-12e) that generates smaller contact stresses on a wider contact area in comparison to a solid damper can be found in the literature. By cutting down the height of the thin-walled damper, its mass can effectively be adjusted for needs of different blade sizes without changing too much the contact stiffness properties. Usually a mass of the under-platform friction dampers can vary from *1 g* (or even lower for special cases) up to several grams.

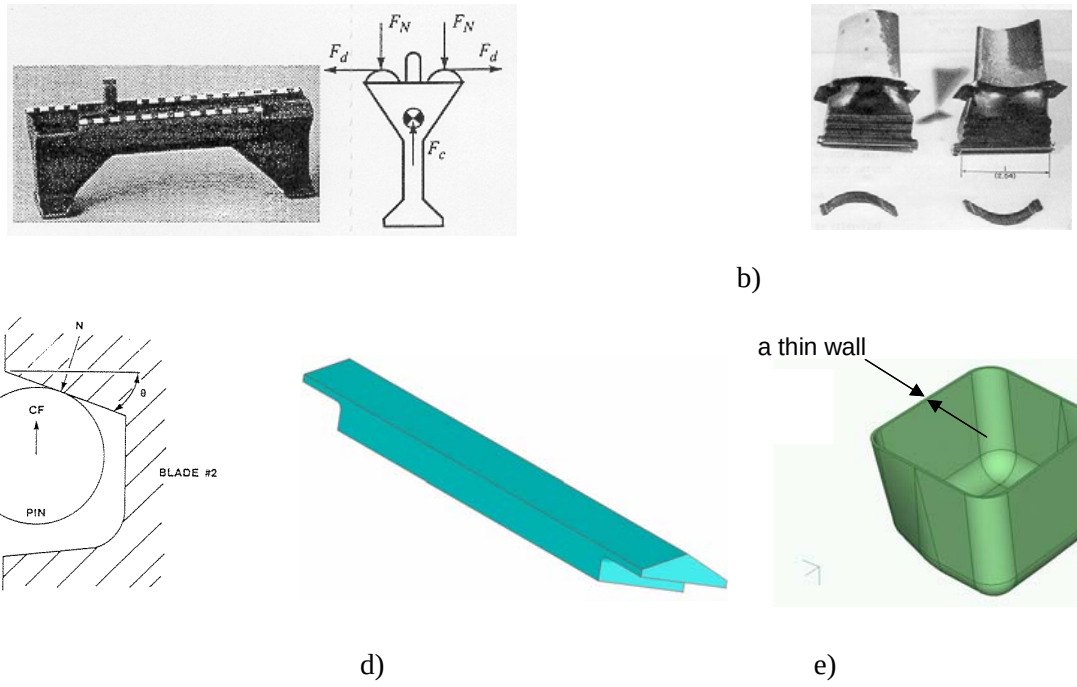

Figure 9-12: Typical under-platform friction dampers used for damping the lowest resonance frequencies of the freestanding blades.

a) Picture of a commercially applied under-platform frictional damper, where white-black strips determine the designed contact area (Csaba, 1998b)

b) A flat under-platform damper in the 1st turbine stage of high pressure fuel turbo-pump of the main engine of the space shuttle (Dominic, 1984)

c) A cylindrical frictional damper used at some Westinghouse blading wheels (Scalzo, 1992)

d) A wedge damper investigated at Imperial College London (Sever et al., 2007)

e) A thin-walled damper investigated at Ecole Centrale de Lyon (Szwedowicz et al., 2006)

According to Panning's experimental and numerical investigations (2005), cylindrical dampers with Hertz's contacts (Figure 9-12c and Figure 9-13a) are less effective than the wedge dampers with flat interfaces because the cylindrical damper contour can roll on the flat contact surfaces of the blades. Indeed, this phenomenon it is known from the classical mechanics, which says that the rolling friction is less resistance in relation to the sliding friction. By considering a wedge damper with flat contact surfaces (Figure 9-13b), the inclination contact angle α has to be correctly determined in terms of the friction coefficient and acting contact forces for prevention of the wedge damper from jamming between the blades. For this reason, asymmetrical wedge dampers with inclination contact angles α and β (Figure 9-13c) are frequently used in bladed discs. For heavy V84.2, V64.3A and V94.3A(2) gas turbine blades, Siemens applies an asymmetrical damper with one curved and another flat contact (Figure 9-13d), whose good damping performances were proved numerically and experimentally under the spin pit and real service condition (Panning et al., 2004). For accelerating the design process of gas turbine blades with asymmetrical dampers, DATAR (Damping of Turbine Blades with Asymmetrical Friction Dampers) program code has been developed at University of Hanover for SIEMENS PG.

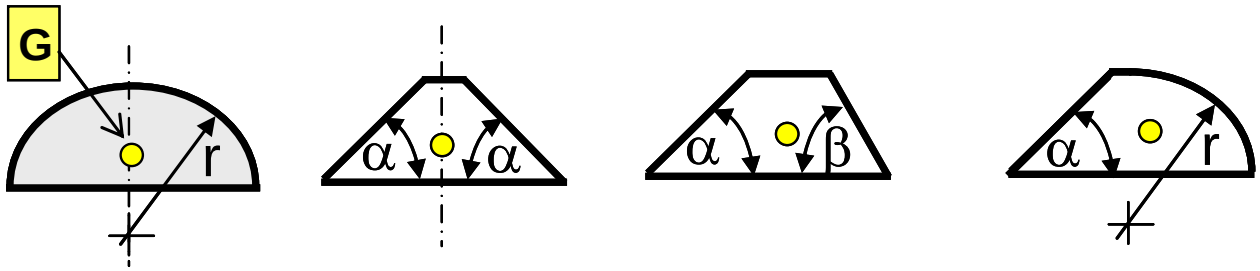

Figure 9-13: Types of the wedge under-platform friction damper, where *G* is the center of gravity of the damper, *r* is radius of the curved contact surface, α and β are contact inclination angles.

If the resonance reaction forces are lower than the threshold friction force on the damper contacts, a damper couples the blades and the blade resonance frequency is higher than that of the blade without damper. This effect is illustrated in Figure 9-14. If the damper mass *m* equals *0*, then the freestanding blade vibrates with its highest length *H* and the airfoil resonance frequency has its lowest value ω_f. Since the mass *m* of the damper is too large and the dynamic reaction forces always are lower than the threshold friction force, the blades are coupled by the dampers. Then, each blade vibrates with its effective length *h* (see Figure 9-14) and the resonance frequency becomes its smallest value ω_c. If the mass of the damper is determined optimally, vibrations of the blade mode shape of interest are effectively suppressed. Then, micro-sliding between the damper and the airfoil contact surfaces occurs, and the effective resonance frequency ω_s of the blade with the micro-sliding damper locates itself between ω_f and ω_c. From the design point of view, the frequency difference $\Delta\omega = \omega_c - \omega_f$ between the freestanding and coupled blade should not differ too much, so that blade resonance would remain in the excitation range of the considered engine order. Panning's (2004) experimental investigation indicates that the fundamental weak bending resonance frequency of the freestanding V94.3A(2) Siemens gas turbine blade increases by *5%* for the cylindrical damper (Figure 9-13a) and by *10%* for the curved-flat dampers (Figure 9-13d).

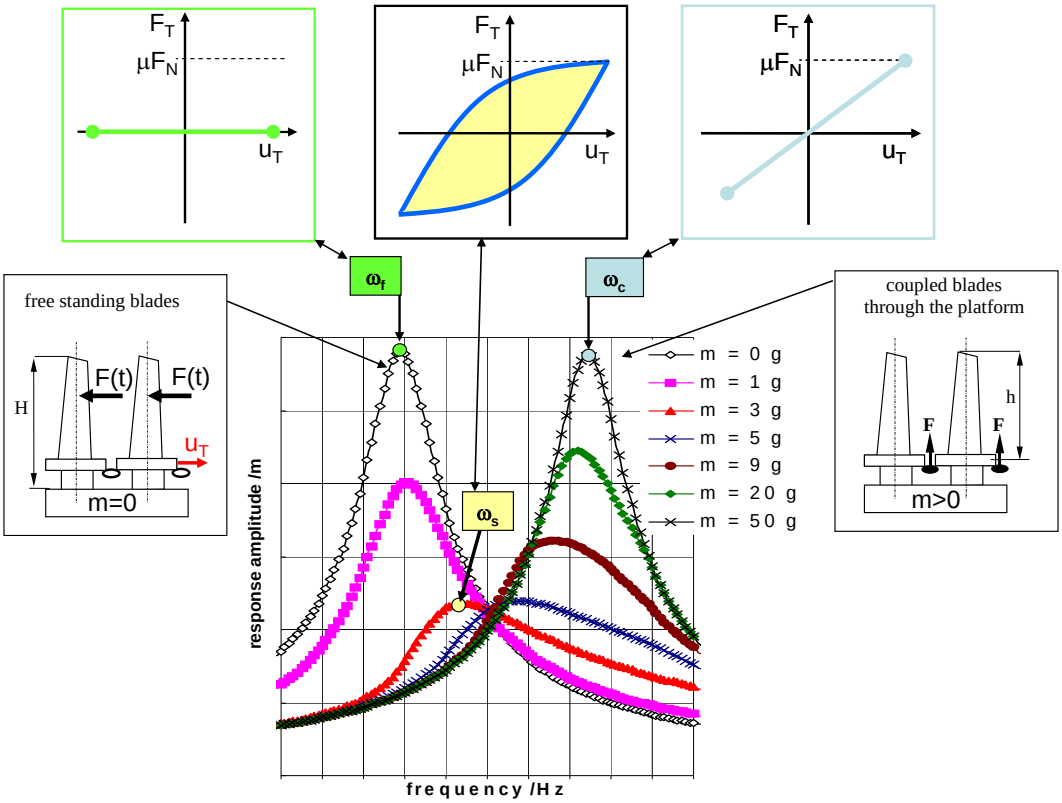

m – mass of the damper,
F – centrifugal load acting on the damper,
u_T – vibration amplitude of the airfoil platform,
F_T – tangential contact stiffness.

Figure 9-14: Resonance response functions of the freestanding blade coupled by the under-platform damper in terms of the damper mass *m.*

The similar resonance behavior can be found for the shrouded blade with respect to the magnitude of the normal force F_N as it is shown in Figure 9-15. Since the normal force is too large, the shroud always couples elastically all blades. For case of too low normal forces, the blades are decoupled from each other at the shroud and each blade would vibrate as the freestanding airfoil. This can lead into rapid fatigue failure (e.g. DiCristoforo and Elledge, 2004). For the shroud connection, it is necessary to find out an optimal value of the normal contact force for the best performance of the friction dissipation of vibrating blades.

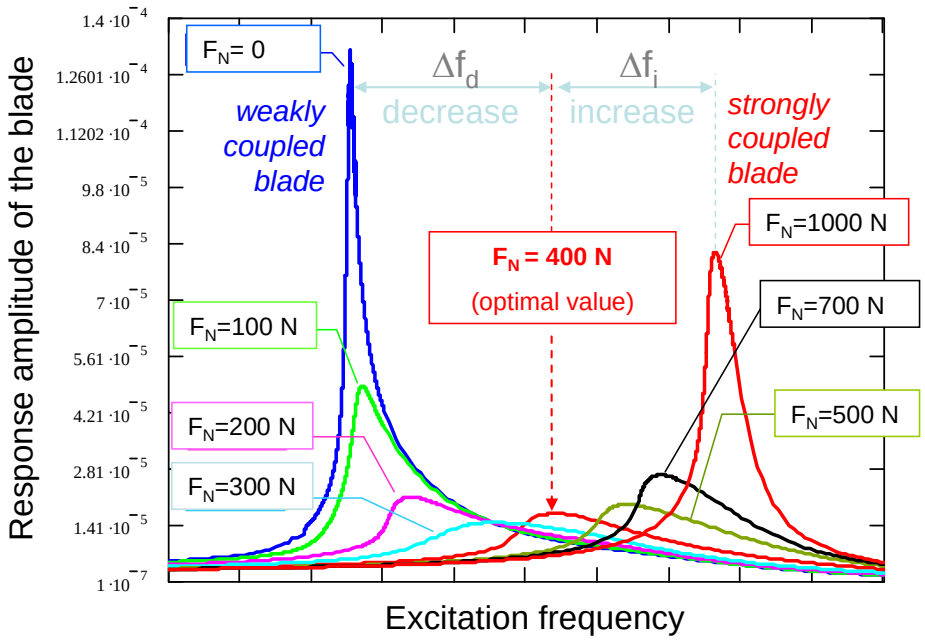

Figure 9-15: Resonance response functions of the shrouded blade in terms of the normal contact force F_N.

Besides the normal contact force, other parameters such as friction coefficient μ, the magnitude of the platform vibration u_T as well as the local contact stiffness C_T, influence on the damping performance for the rotating blades. An understanding of the influence of these four major parameters on the hystersis frictional loop is explained in Figure 9-16.

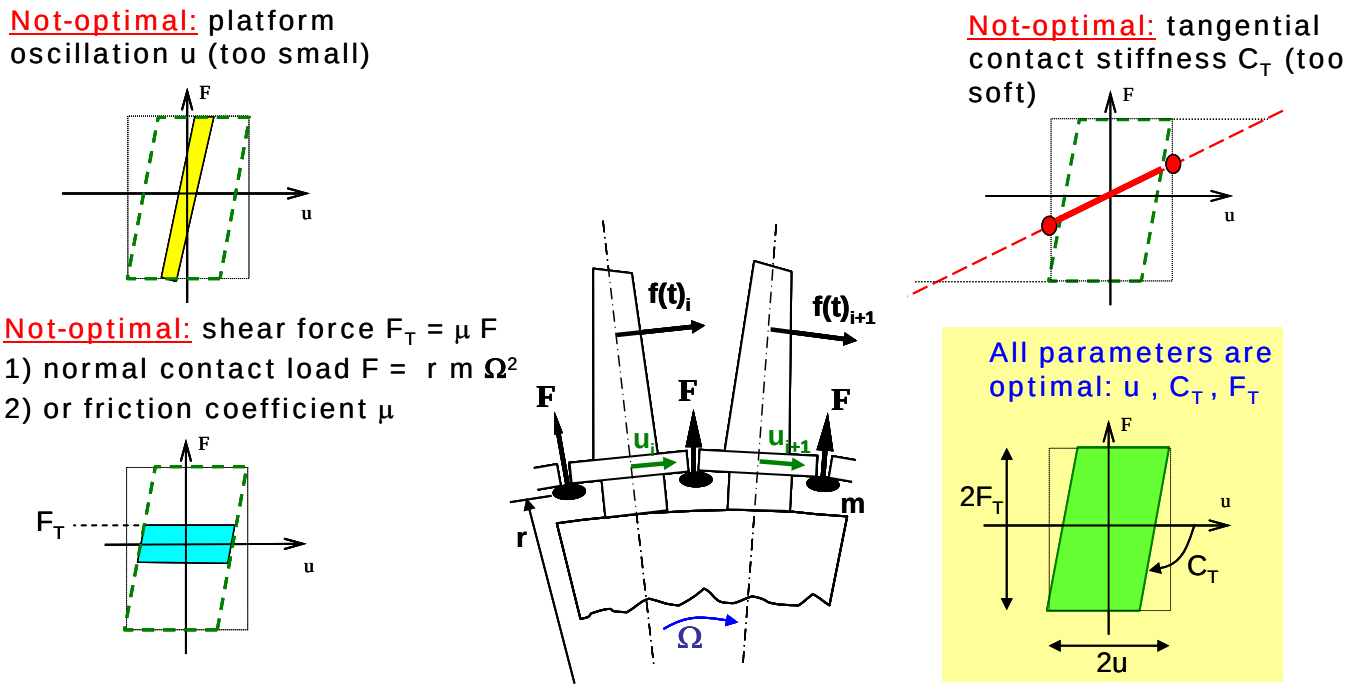

Figure 9-16: Influence of the damper mass m, rotational speed Ω, the radial position of the damper *r*, friction coefficient μ, the local tangential contact stiffness C_T and response tangential amplitude of the contact surface (without damper) u_T on the damping performance.

If vibrations of the blade platform u_T are too small, what means that the blade shank is not enough flexible, the friction damper would not slip as much as it is possible for getting the highest damping performance (see Figure 9-16). The threshold friction (shear) force depends on the damper mass m, the rotational speed Ω, radial position r of the damper within the bladed disc and on the friction coefficient μ. Since the threshold contact force F_T is too small, the hystersis frictional loop does not reach its possible optimal amount, as it is shown in Figure 9-16 (see the left lower hystersis frictional loop). Finally, the local tangential contact stiffness C_T affects the friction damping performance (see the right upper hystersis frictional loop in Figure 9-16). Since the elastic local deformation between the airfoil surface and the damper contour is too large, the damper can only couple elastically the blades and the frictional slipping might never be generated on the contact. In reality, the local elastic deformation between the damper and airfoil always occurs, although the lowest eigenfrequencies of the unrestrained damper are much higher the blade eigenfrequnecy, which is considered for the frictional damping. The engineering sense of the local tangential contact stiffness C_T is explained in Figure 9-17. Multiplying the local tangential contact stiffness C_T by relative deformations $u_{T,j}$ and $u_{T,j+1}$ of the adjustment blade platforms j and $j+1$ the tangential reaction on the contact is generated. This force allows for damper sliding, if it is bigger than the threshold friction force μF_N. Then, this slip condition can be expressed by

7) $C_T \left(u(t)_{T,j} - u(t)_{T,j+1}\right) \geq \mu F_N$, then the damper slips on the contact, where t denotes time.

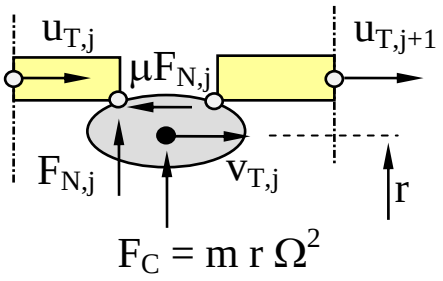

Figure 9-17: Engineering sense of meaning of the local tangential contact stiffness C_T for slipping of the friction damper, where deformations $u_{T,j}$ and $u_{T,j+1}$ of the adjustment blade platforms *j* and *j+1*.

In equation (7), the relative deformation $\Delta u(t)_{T,j} = u(t)_{T,j} - u(t)_{T,j+1}$ of the adjustment blades *j* and *j+1* influences significantly the damping performance of the damper. Considering the tuned blades in the turbine stage coupled additionally by an elastic disc, the damper hypothetically does not produce any friction dissipation when the blade disc vibrates with the *0*-th nodal diameter. For this case, all blades vibrate with the same phase along the circumferential direction. But the damping performance of the damper continuously grows with higher number of the nodal diameter number. Its highest performance theoretically is obtained for the out-of-phase mode shape of the disc vibrating with nodal diameter number $n = N^*/2$, where $N^*=N-1$ or $N^*=N$ for the odd or even number *N* of the blades in the stage, respectively. In reality, the blades are mistuned and the damping performance of the damper also can be noticed for the lowest nodal diameter numbers.

The engineering process of the blade designing exploiting of the friction dissipation is complex numerical analysis. As it is shown in Figure 9-18, this process needs to be based on the special numerical tool, which uses data from the FE simulation, measurements of the friction coefficient, wear rate and other contact parameters, like surface roughness. Although some of these design tools (for instance Petrov's code, 2007) are able to consider many details of the dynamic contact behavior with variable normal contact forces and contact roughness as well as mistuning of blades, the engineer must always face up different uncertainties due to the real contact behavior and unknown excitations acting on the blades. These aspects will be considered further in this report. However, the fundamental role of thumb says that before beginning the entire designing process, the vibration ratio between the airfoil tip and the platform needs to be proved firstly. Since this vibration ratio of the platform deformation $u_{PLATFORM}$ to the deformation of the airfoil tip u_{TIP} (see Figure 9-18) is less than *9*, then considerable high damping performance can be achieved.

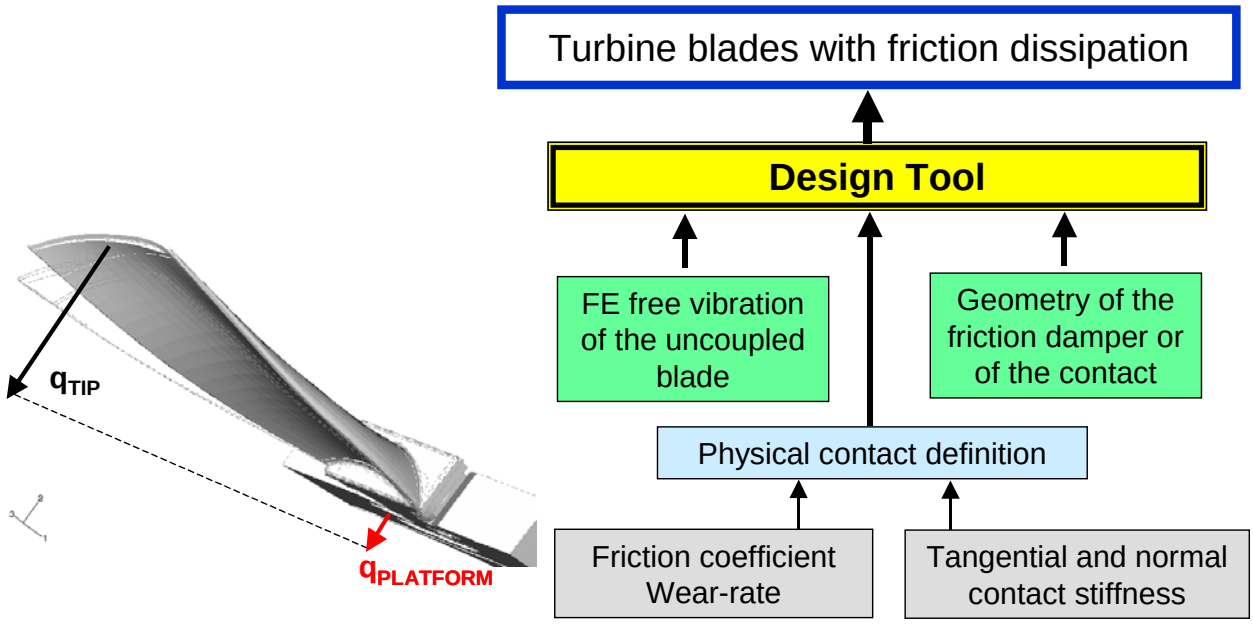

Figure 9-18: The engineering process of the blade designing considering the frictional dissipation based on the dynamic synthesis and the harmonic balance method.

The friction damping technique is based on micro-sliding on the contact, which can lead to fretting fatigue. The fretting wear and corrosion are avoided usually by using proper oxide coatings, which are proved by a series of fretting experiments (Swikert and Johnson, 1968).

4.0 REFERENCE BENCHMARK OF THE BLADE DYNAMICS WITH FRICTION DISSIPATION

The here presented methodology for the numerical analysis of the blade dynamics with friction is considered for the last low pressure (LP) steam turbine blades with friction bolts (Szwedowicz et al., 2008a and 2008b), which were designed at Siemens PGI in the 80s. This is a straightforward approach considering engineering needs in the design process of the blades with friction at shrouds, winglets, bolts, lacing wires or under-platform dampers including the elastic disc coupling. The whole numerical process is done for the tuned disc assemblies.

For computations of nonlinear forced blade vibrations with frictional sliding, the DATES code is applied here. This program allows for analyzing friction dissipation on contacts of a shroud, a winglet, a wire and an under-platform. Its solution technique of the non-linear dynamics is based on the linearization of friction forces with one Fourier component by using the harmonic balance method. Thus the frictional hystersis loop is represented with the elliptical form as shown in Figure 9-5a. The development of this code was supported within industrial-government consortia FVV[1] at University of Hanover (Sextro, 2002, Panning, 2005) in Germany.

[1] FFV - Forschungsvereinigung Verbrennungskraftmaschinen

The last LP steam turbine SK-stage has strongly twisted and tapered blades as it is shown in Figure 9-10. The airfoil is bolted to the rotor through *4* fingers of its radial root with *2* conical pins (Figure 9-10a). In the upper airfoil part, bolts with conical ends are loosely fitted within the cylindrical hollows of adjacent blades. By increasing the rotational speed, *N* blades are coupled by these bolts. They can operate as friction dampers, in case that the excitation exceeds the threshold friction forces F_μ between the bolt and the airfoil. Then, resonance stresses of the SK-blades operating with variable rotational speed are effectively reduced below the maximum allowable value. For the 1st frequency family, this damping capability of the smallest SK-blades was experimentally developed and validated at the set-up of the real turbine unit at the Stuttgart University in the early 80s by Wolter (1980), Figurski (1981, 1992), Beckbissinger (1982), and Pfeiffer (1985). The experimental results of the dynamic and damping behavior of these blades are well summarized by Wachter et al. (1983). Disc vibrations were measured with *12* gauges placed at position *A* of *12* adjacent airfoils (Figure 9-19). This gauge location was determined by Wolter (1980) for the freestanding blade. Between *4500* and *15000* rpm, the blades with bolts were investigated for different mass flow and back-pressure indicated by tests *A*, *B*, *C*, *D* and *P*, considering resonant stresses of the 1st eigenfamily, which are shown in Figure 9-19c. In all these tests, double resonances ω' and ω" were measured, what relates to *2* standing vibration waves in the mistuned disc assembly.

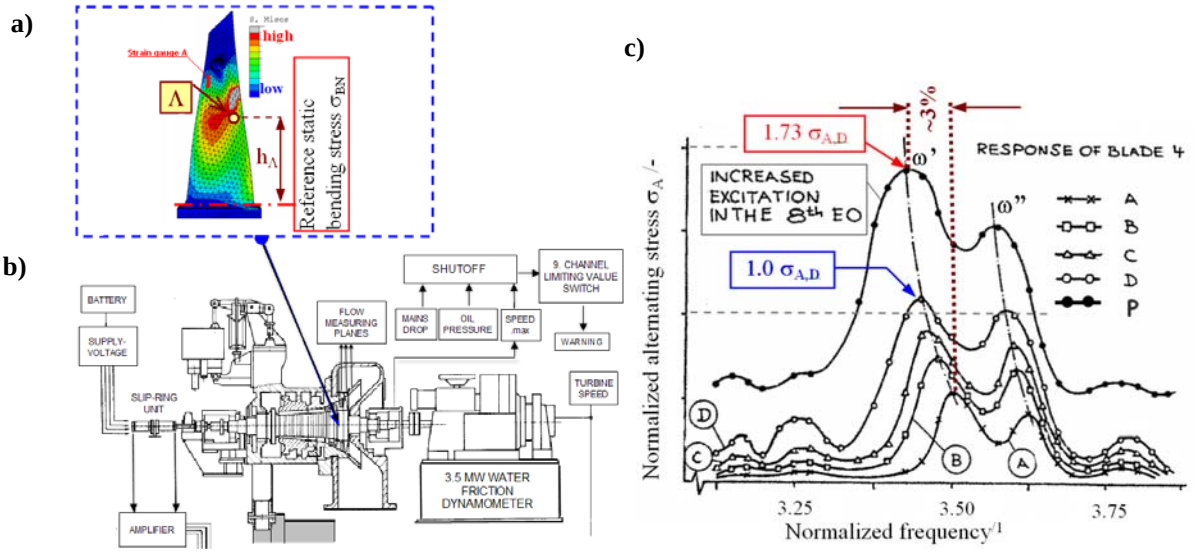

Figure 9-19: a) FE static bending stresses of the last low pressure steam turbine SK-blades at the nominal speed Ω_n, where Λ is position of the resulting excitation force at the radius h_A, b) the test rig with the SK-turbine at the Stuttgart University (Wachter et al., 1983), c) Variation of the order tracking of the 8th engine order of the 1st resonance frequencies at blade *4* for different service conditions *A*, *B*, *C*, *D* with full steam loading and *P* with partial arc admission, where ω' and ω" are resonance amplitudes of the mistuned bladed disc.

In the dynamics of SK-blades, the friction dissipation at the radial root is neglected regarding the minor disc influence on blade vibrations and insignificant mode shape oscillations in the lower part of the blade (Szwedowicz et al., 2008a). For different mass flow conditions between tests *A* and *P* (see *3%* difference between resonance frequencies $\Delta\omega = \omega'_P - \omega'_A$ in Figure 9-19 and dashed-pointed lines), the identified frequency shifting proves the presence of friction dissipation on the bolt contacts (see explanation in Figures 9-14 and 9-15). Therefore, the dynamic reactions and friction forces $F(t)_\mu$ have to be included in the SK-blade vibrations.

At the rotational speed Ω, temperature *T*, and friction coefficient μ, the static blade deformations and reaction forces at the bolt contact regions are obtained from the cyclic FE model. The FE contact area and resulting

forces R_{S3} and R_{P3} are illustrated in Figure 9-7. The expected elliptical contact area $A=\pi a_o b_o$ has to be approximated with the equivalent rectangular contact area $A=ab$ (Figure 9-3) because of some restrictions and simplifications in the applied software.

Periodic blade vibrations with friction bolts are described with the cyclic symmetrical hypothesis and the component mode synthesis. For the computational accuracy, the frequency response functions (FRF) of the bladed disc have to be represented at least with *15* FE mode shapes, as it was proved for the shrouded blade by Treyde (1994). Because the natural frequencies of the unconstrained friction bolt are far away from the frequency range of interest (see Figure 9-11), flexibility of the damper is not essential for reliable computations and it is modeled here as a rigid coupling element.

The cyclic FE dynamic equations of the tuned disc assembly, whose *n*-th nodal diameter number is excited harmonically by engine order *k*, are expressed in the time domain *t* as

$$8)\quad \left[M\left(e^{jn\varphi}\right)\right]\{\ddot{w}_n\}+[D]\{\dot{w}_n\}+\left[K\left(e^{jn\varphi}\right)\right]\{w_n\}=\{F_k\}e^{jk\Omega t}+\{F(t)_C\},$$

where the Rayleigh damping matrix *[D]* is defined by a linear combination of the mass $[M(e^{jn\varphi})]$ and stiffness $[K(e^{jn\varphi})]$ matrices depending on the cyclic sector angle $\varphi=2\pi/N$ and nodal diameter $n = 0, 1, 2, \ldots, (N-1)/2$ for the odd number N of the analyzed blades. In the modal domain for the excitation orders of interest, the proportional damping matrix *[D]* is redefined with the modal damping ratios ξ, which are known from the experiment. The generalized complex vector $\{w\} = \{\{z\},\{q\}\}^T$ describes vibrations of the internal nodes $\{q\}$ and external nodes $\{z\}$ located on the cyclic boundaries of the FE model (Szwedowicz et al., 2008a). In terms of excitation magnitude, the generalized vector $\{F(t)_C\}$ contains either two tangential $R(t)_s$ and one normal $R(t)_n$ contact reaction forces for sticking contact condition or two friction forces $F(t)_\mu$ and one normal reaction force $R(t)_n$ for sliding contact condition at the bolt. For the high centrifugal load acting on the bolts, the contact separation ($F(t)_n < 0$) should not occur for the analyzed 1^{st} blade eigenfamily. In simulations, the separation is proved by validation of the load equilibrium on the contact regarding a negative resulting normal force as undesired results from the design point of view. Then, the mass of the bolt needs to be increased for preventing it from possible impacting effects in the contact region, which can induce fretting fatigue (Szwedowicz et al., 2005).

For the considered harmonic excitation, the blade response is treated also as harmonic vibration by representing the periodical non-linear friction forces $F(t)_\mu$ with the complex Fourier series. This HBM linearization is applicable for weak non-linearities, which depend on the frictional hysteresis determined by both velocity and displacement of the contact point. For the simplicity, only the fundamental Fourier coefficient is taken into account, which assures a conservative assessment of the minimum friction dissipation on the contact. By application of more Fourier coefficients (Wang and Chen, 1993, Petrov, 2006), the real shape of frictional hysteresis can be determined more exactly, instead of the elliptical form obtained with one complex Fourier coefficient (see Figure 9-5b). Besides the main blade resonance $\omega_{i,n}=k\Omega$ as it is calculated for the fundamental Fourier harmonic, the utilization of higher numbers of the Fourier harmonics predicts also the sub- and super-harmonic responses due to contact non-linearity (Petrov, 2006).

In the design process, the blade mistuning is not a deterministic quantity and therefore, the tuned system of the blades is taken into account. Then, according to the orthogonal condition between the disc mode shape and excitation form, the blade resonances with the satisfied condition $k=n$ are considered only. By applying the modal transformation to equation (8), the blade dynamics with the linearized contact forces are reduced to modal equations of *n*-th nodal diameter vibration as

9) $h_{i,n,k}\ u_{i,n} = f_{i,n,k} e^{jk\Omega t} + \{\Phi^o\}_{i,n}^{*T} \{f_c(\Delta u_{i,n})\}_{i,n}$, ,

where $()^{*T}$ denotes the conjugate transposed complex mode shape vector $\{\Phi^o\}_{i,n}$ and $f_{i,n,k}$ is the modal force, which is expressed as

10) $f_{i,n,k} = \left\{\Phi^\circ\right\}_{i,n}^{*T} \{F_k\}.$

In equation (10), index *i.n* means the disc mode shape of the *i*-th eigenfamily vibrating with the nodal diameter *n* and $\left\{\Phi^\circ\right\}_{i,n}^{*T}$ is the conjugate transposed vector of the FE mass-normalized mode shape $\{\Phi^\circ\}_{i,n} = \{\phi^\circ_{i,n}\}_c + j\{\phi^\circ_{i,n}\}_s$, of the blade represented by the cyclic FE model. The parameter F_k is the excitation amplitude of the *k*-th engine order. In equation (9), the modal dynamic stiffness $h_{i,n,k}$ is given as

11) $h_{i,n,k} = -(k\Omega)^2 + j2\omega_{i,n}\xi_{i,n}k\Omega + \omega_{i,n}^2.$

The contact force f_c in equation (9) depends on the relationship $\Delta u_{i,n}$ between the blade and the bolt modal displacements on the contact, as it is determined by Siewert et al., (2006). The here used theory is explained in detail by Sextro (2002) and is based on the harmonic balance method and the dynamic synthesis. The FE elliptical contact area is simplified by the equivalent rectangular shape $a \times b$ (Figure 9-7) for the contact discretisation on each end of the bolt. Each contact area is represented with *100* $\eta \times \zeta$ contact points (where $\eta = 10$ and $\zeta = 10$). At each contact point $\eta_\iota \times \zeta_\iota$ three contact conditions are possible, such as: slipping, sticking or separation. This discretisation allows predicting local micro-slips, stick-slip, stuck and separation in different regions of the contact. The local contact stiffness and contact forces at each ι-th contact point $\eta_\iota \times \zeta_\iota$ are obtained from the resulting normal C_N and tangential C_T contact stiffness and resulting FE reaction forces R (see e.g. point C_s in Figure 9-7) by using the multi-point constraints. Applying the kinematic constraints, the initial spatial motion of each contact point ι is determined from the oscillations of the resulting contact point C_S or C_P (Figure 9-7), which are known from the FE free vibration calculation.

Because the fundamental natural frequency of the unconstrained bolt is *40* times higher than the 1st blade eigenfrequency (see Figure 9-11), the bolt is considered as a rigid body for the analyze of the 1st eigenfamily vibrating with nodal diameters between *6* and *13* according to the Campbell diagram. Then, *6* rigid body motions of the bolt are used in the modal simulations.

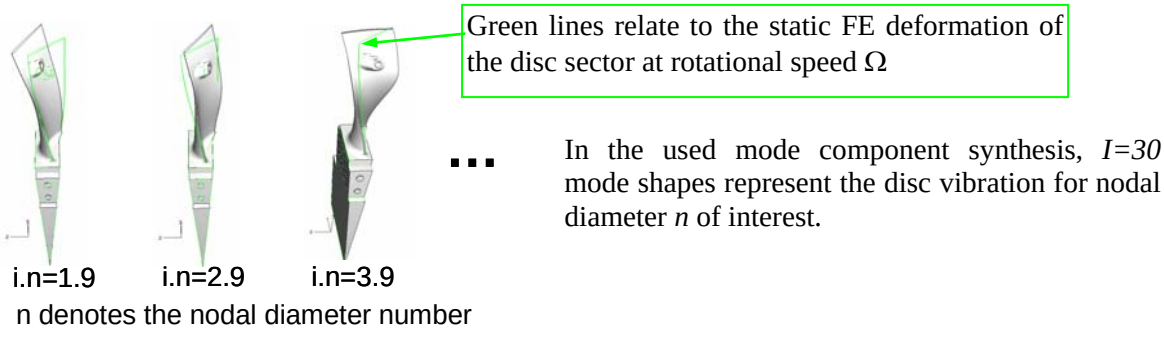

Figure 9-20: Illustration of the *3* lowest mode shapes of the blade without bolt coupling used for the modal transformation of the FE disc vibrations of the nodal diameter *n=9*.

The modal steady-state response analysis is performed with a sweep excitation for a chosen frequency step $\Delta\Omega$ of interest. The computation starts from frequency Ω_{lower_band} and is completed at the end frequency Ω_{upper_band}, where $\Omega_{lower\_band} < k\Omega < \Omega_{upper\_band}$. For each excitation frequency $\Omega_e = \Omega_{lower\_band} + p\Delta\Omega$, where $p = 0, 1, 2, \ldots, (\Omega_{upper\_band} - \Omega_{lower\_band})/\Delta\Omega$, the non-linear modal dynamic equation (9) is solved by using the Newton-Raphson method (Kelley, 2003). The blade dynamic stress σ_n, strain ε_n or displacement w_n amplitudes are determined by the transformation of the calculated complex modal responses $u_{i,n}$ into the Cartesian system as

$$12)\quad \{w(t)\}_n = \sum_{i=1}^{I} \{\phi^o\}_{i,n} u_{i,n} \exp(-j\Omega_e t)\ ,\ j = \sqrt{-1}$$

The entire modal non-linear dynamic analysis is very efficient in practical application. Using ordinary computers any order tracking of the specified n-th nodal diameter (e.g. see Figure 9-19c) is computed in a short time within the frequency range of interest for the known excitation force, friction coefficient and the resulting contact stiffness C_N and C_T.

4.1 Determination of the Local Contact Stiffness

The determination of the local contact stiffness is very essential aspect for reliable simulations of the blade vibration with friction dissipation. For the contact stiffness assessment, *4* approaches are known in the literature which are based on

i) The analytical solution,

ii) The non-linear FE analysis,

iii) The residual stiffness analysis, and

iv) The FE-modal contact adjustment.

The **analytical manners** are limited to the circular or elliptical contact areas, which are calculated with the Hertz's (1882) or the Catteano-Mindlin theory (Balmer, 1992), respectively. The shape of the contact area is unlimited in the **non-linear static FE methodology** of the stiffness contact computation proposed and validated in by Szwedowicz et al., (2001 and 2006). In this method, although a very fine FE mesh is used for the contact representation, the stiffness values usually are overestimated in relation to the experimentally results of about *6-11%* because of the neglected surface roughness as well as adhesive contact and viscous-elastic solid behavior. Figure 9-21 shows the comparison of the experimental stiffness evaluated from the measured hystersis frictional loop with the two-dimensional FE results of the specimen with the Hertz's contact. For friction coefficients of *0.5* and *0.7* known from the quasi-static measurement, the numerically determined tangential contact stiffness values are overestimated for ambient as well as for the evaluated temperature between *400°C* and *600°C* (Figure 9-21c). By an increase of the temperature, the contact stiffness reduces as it is confirmed by the measurements in Figure 9-21c.

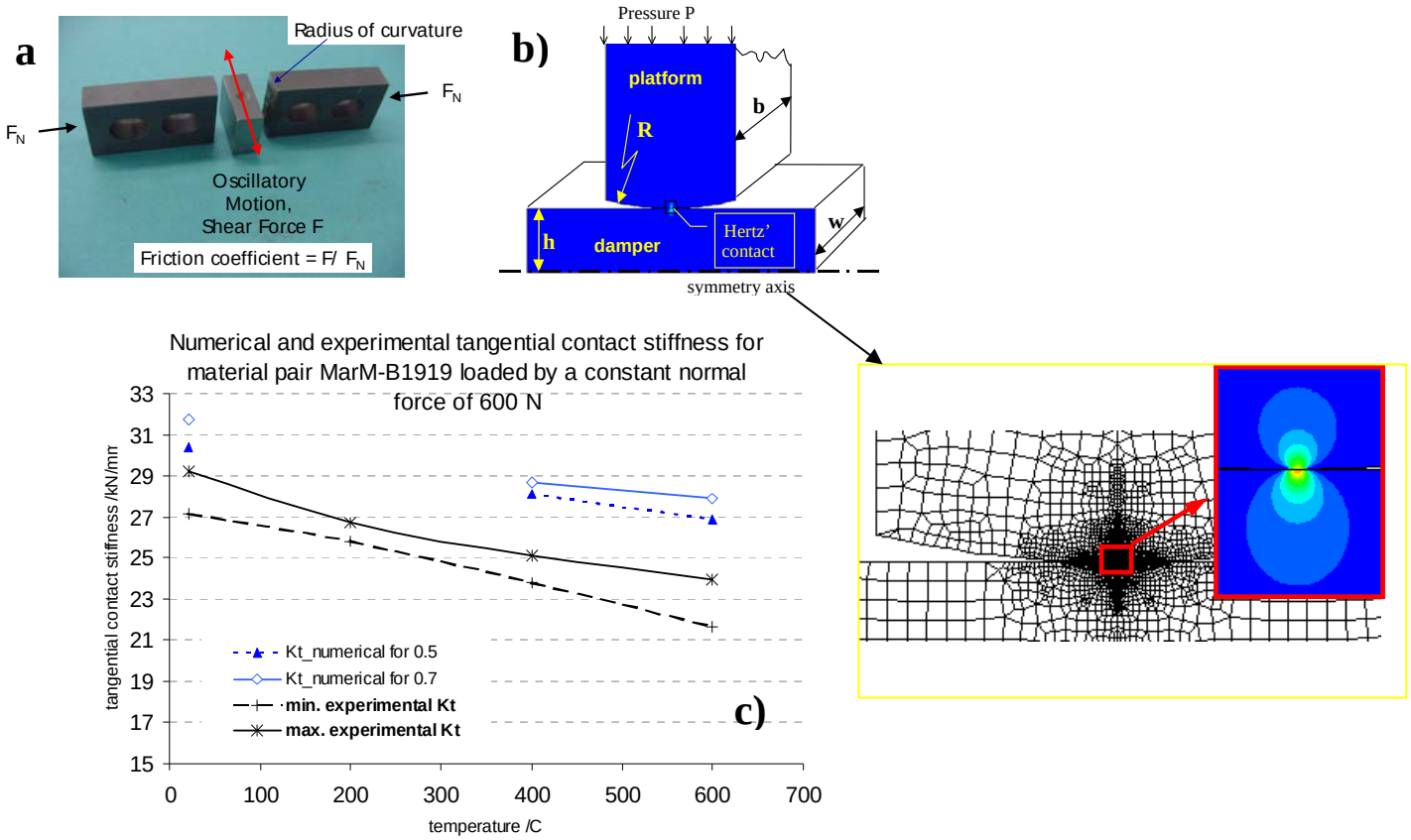

Figure 9-21: Specimen (a), 2D FE model (b) and the comparison of the calculated contact stiffness for friction coefficients of *0.5* and *0.7* with the experimental data (c) measured at the ALSTOM set-up for quasi-static tests.

The evaluation of the experimental contact stiffness from the measured hystersis frictional loop is explained in Figure 9-22a. Figures 9-22b illustrates the methodology for the FE computation of the contact stiffness. Firstly the centrifugal load is applied to the damper and the platform to find the contact area for the specified friction coefficient. For the calculated deformed state, a small virtual acceleration G_N in the normal direction n is firstly applied incrementally to the damper. By increasing the acceleration, at each numerical increment i corresponding to the increase of the acting load, the normal reaction force $R_{N,\kappa,i}$ and normal contact deformation $u_{N,\kappa,i}$ are obtained at each node κ, which is in contact with the platform. At the numerical increment i, the nodal contact stiffness $k_{N,\kappa,i}$ at node κ in the sticking contact is determined from

$$13)\quad k_{N,\kappa,i} = (R_{N,\kappa,i} - R_{N,\kappa,i-1}) / (u_{N,\kappa,i} - u_{N,\kappa,i-1}).$$

For all nodes K in contact, whose number varies depending on the magnitude of the centrifugal load and the elastic damper deformation, the parallel arranged virtual normal springs represent these elastic behavior. The total normal contact stiffness $C_{N,i}$ is then found at each FE increment i as

$$14)\quad C_{N,i} = \sum_{\kappa=1}^{K} k_{N,\kappa,i}\ .$$

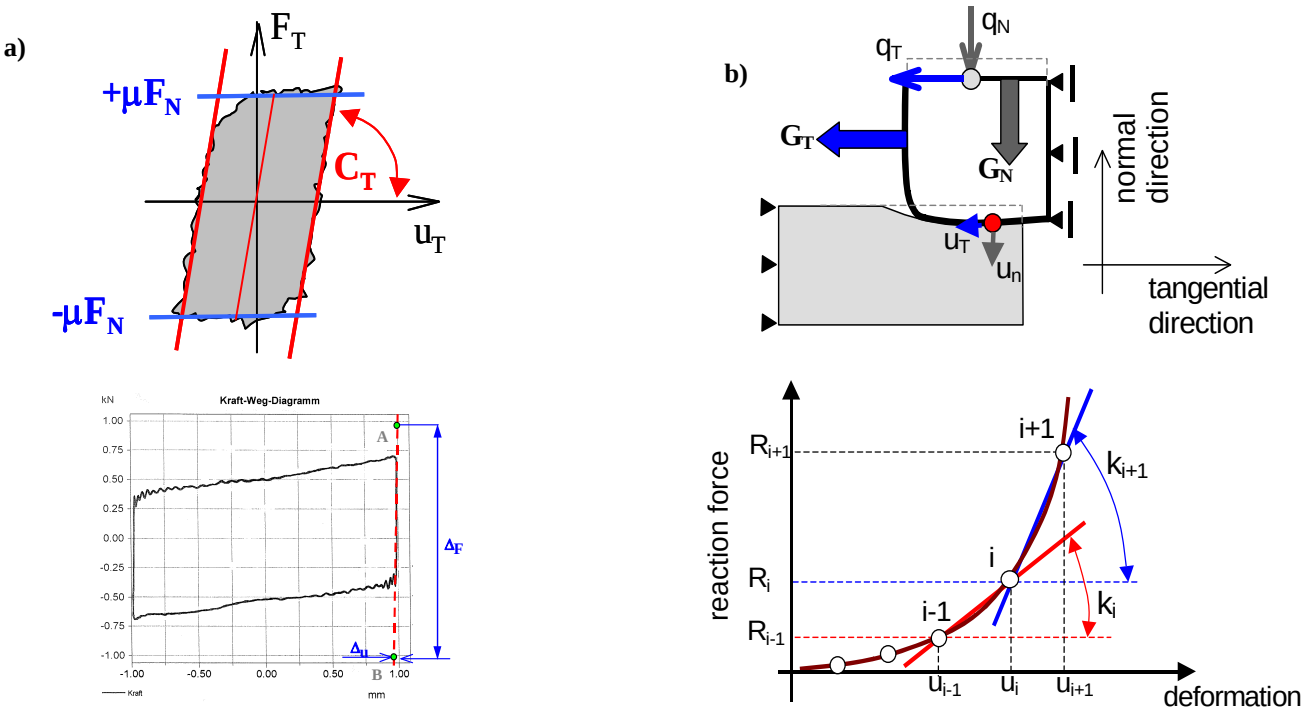

Figure 9-22: a) Evaluation of the contact stiffness from the measured hystersis frictional, b) Numerical manner for the computation of the contact stiffness.

By applying a virtual acceleration G_T (Figure 9-22b) in tangential direction t to the damper, very small tangential deformations of the damper in contact with the platform are induced for an assumed friction coefficient. For the tangential reaction force $R_{T,\kappa,i}$ and tangential contact deformation $u_{T,\kappa,i}$, the tangential contact stiffness $k_{T,\kappa,i}$ at node κ in contact is determined in the same manner as the normal contact stiffness $k_{N,\kappa,i}$ from

$$15)\quad k_{T,\kappa,i} = (R_{T,\kappa,i} - R_{T,\kappa,i-1}) / (u_{T,\kappa,i} - u_{T,\kappa,i-1}),$$

where i denotes a numerical increment of the non-linear FE solution of the contact problem. The obtained nodal tangential springs at all nodes K in contact are in serial arrangement and the total tangential contact stiffness $C_{T,i}$ is found at each FE increment i from

$$16)\quad \frac{1}{k_{t,i}} = \sum_{\kappa=1}^{K} \frac{1}{k_{t,\kappa,i}}.$$

In Figure 9-23, the FE results of the computed contact behavior of the cylindrical friction damper are presented, which are used for the evaluation the tangential contact stiffness C_T. The sensitivity of the tangential contact stiffness of the same damper in terms of the friction coefficient and the radius of the damper outer contour is given in Figure 9-24.

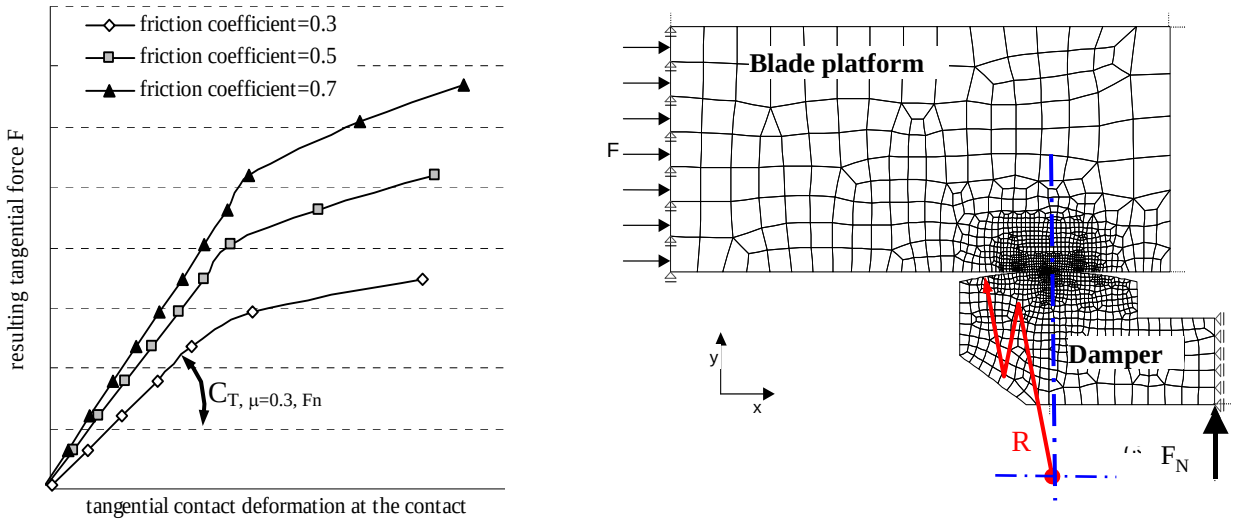

Figure 9-23: Numerically computed stiffness sensitivity of the cylindrical friction damper in terms of the normal contact force FN and radius R shown in Figure 9-23.

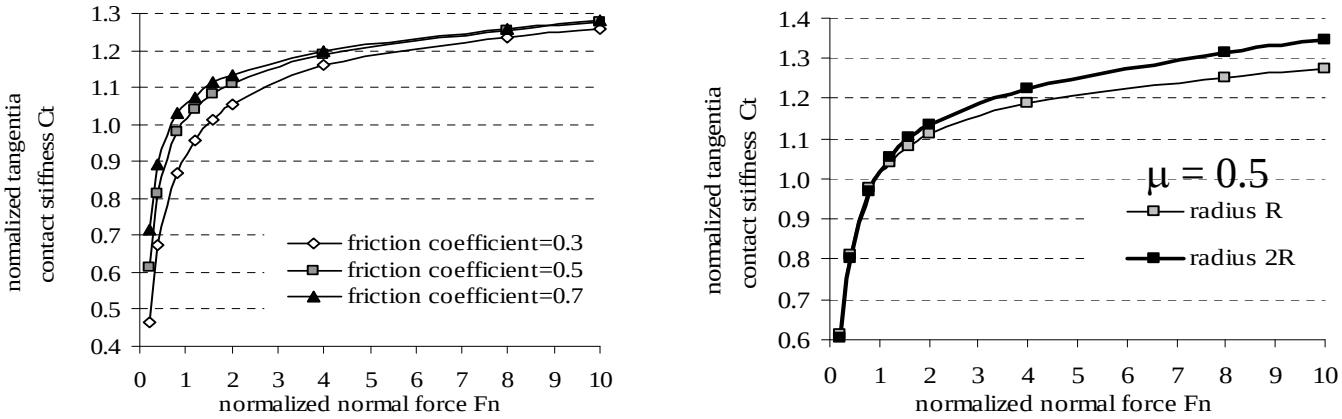

Figure 9-24: Numerically computed sensitivity of the contact stiffness of the cylindrical friction damper in terms of the normal contact force F_N and radius R shown in Figure 9-23.

For the correct prediction of the static blade deformation in the modal domain by using *I* number of mode shapes, **the residual stiffness method** is introduced by Sextro (2002). The same pressure is imposed on the contact area of both uncoupled blade in the FE model and the modal blade model (equation 9). Then, the quasi-static contact deformations are calculated with the non-linear modal model for an excitation Ω_{lower_band} of about *1* Hz. The same is done with the FE model. Finally, the residual stiffness is calculated by relating both solutions to each other. More details of this process are described in Siewert et al. (2006).

Here, the **FE-modal stiffness adjustment approach** is used, which is proposed by Szwedowicz et al. (2005, 2006, 2008b). This analysis is based generally on the well-known 1D characteristic of disc vibrations. Firstly

the initial normal $C_{N,o}$ and tangential $C_{T,o}$ contact stiffness values between the damper and airfoil are estimated with the Hertz's formulas. For the neglected friction dissipation and the sticking contact condition, the modal nodal diameter curves are computed by solving equation (9) for the estimated contact stiffness $C_N = C_{N,o} \pm \Delta c_N$ and $C_T = C_{T,o} \pm \Delta c_T$ (see Figure 9-25). Then, the modal and FE nodal diameter curves are compared to each other. If the discrepancy between the FE and modal resonance frequencies is above the allowable relative error, the computation of the modal diameter curves is repeated again for new $\pm\Delta c_N$ and $\pm\Delta c_T$ values.

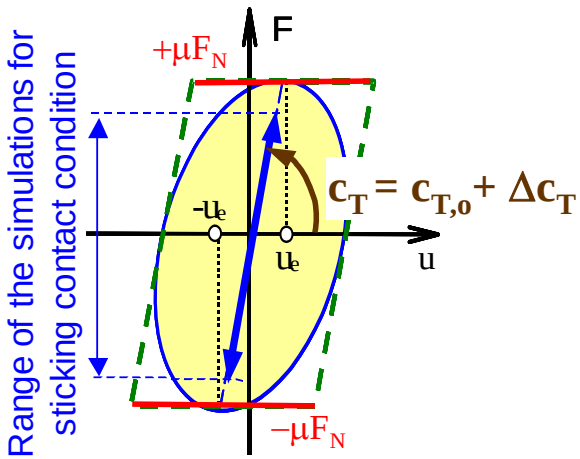

Figure 9-25: Graphical illustration of the methodology principle for the FE-modal stiffness adjustment.

For the here considered blade with friction bolts, this iterative process delivers finally the resulting contact normal and tangential stiffness $C_{N,S}$ and $C_{T,S}$ at the left and $C_{N,P}$ and $C_{T,P}$ at the right contact points C_S and C_P of the bolt (Figure 9-7). According to the comparison of the experimental and numerical results for the shroud coupling as well as for the under-platform damper, the non-linear FE and the FE-modal contact adjustment method predict contact stiffness values in the reliable manner especially for the lowest eigenfamilies of the bladed disc. As it is proved by Siewert et al. (2006), its application in the non-linear blade dynamics delivers a better agreement with the measured resonance frequencies and resonance amplitudes than e.g. the residual stiffness approach. The application of this approach is illustrated for the friction bolt coupling in Figure 9-26 and for the shroud coupling in Figure 9-27. For the determined contact stiffness for the sticking contact condition (see explanation in Figure 9-25), the maximum errors of *1.2%* and *4%* are found for the shroud and bolts, respectively. More details about these analyses can be found in Szwedowicz et al. (2005) and (2008b). In general, as it is shown in Figures 9-26 and 9-27, the contact stiffness values for these both couplings differ significantly to each other.

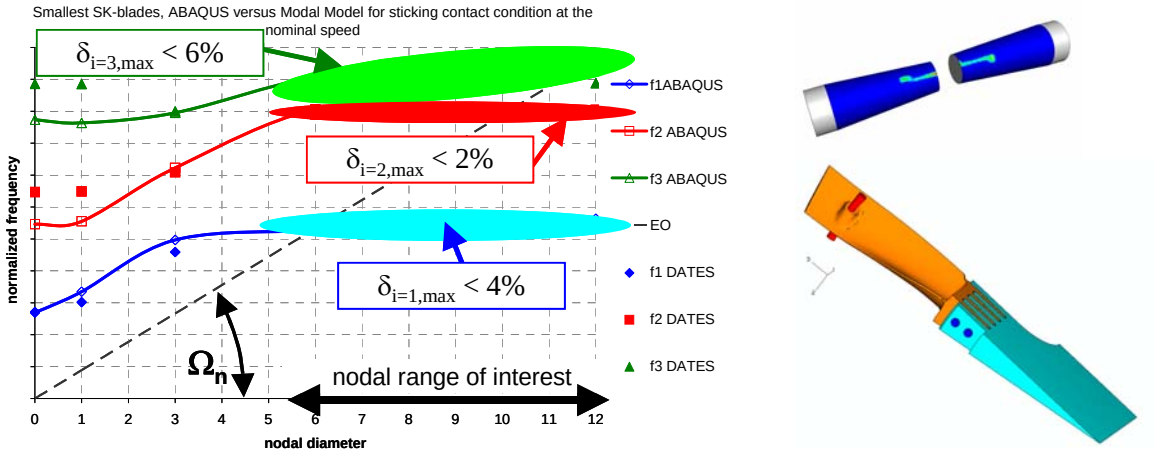

Figure 9-26: For the nominal speed ABAQUS results and DATES nodal diameter curves for the adjusted tangential C_T = *29 MN/m* and normal C_N = *59 MN/m* contact stiffness at the friction bolts assembled loosely in the blades (Figure 9-7).

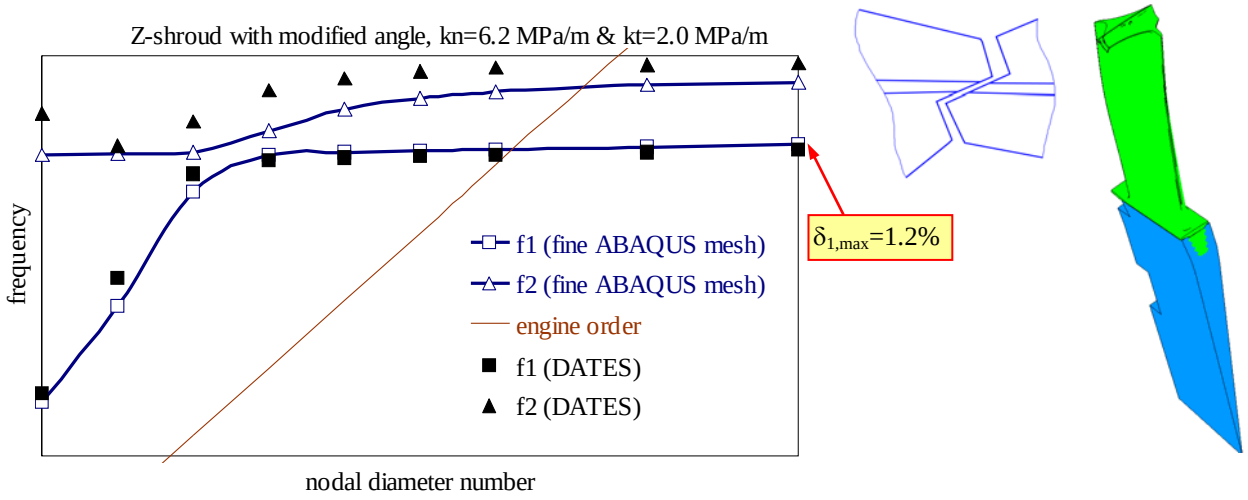

Figure 9-27: For the nominal speed, ABAQUS results and DATES nodal diameter curves for the adjusted tangential $k_t = C_T$ = *2.0 MN/m* and normal $k_n = C_N$ = *6.2 MN/m* contact stiffness at the Z-lock shrouded blades, which are assembled together with clearance at standstill.

4.2 Assessment of the Overall Damping Acting on the Blade

The friction damping is an additional dissipation source in the overall damping acting upon the blade. The vibrating damping is damped mainly by aerodynamic viscous and hysteretic (material) dissipation. The material damping depends generally on alloy properties, temperature and the magnitude of the normal dynamic stresses in the vibrating blade. Figure 9-28 shows experimental modal damping ratios for different alloys, which were measured by Schmidt (1962). The highest damping values are for X20Cr13 and X22CrMoV12.1 alloys. For other alloys, the material modal damping ratios are below *0.08%*, when the

dynamic stress magnitude reduces below *100 MPa*. For rotating components, which experience high mean stresses, the material damping is negligible small and usually its dissipation meaning is omitted in the design consideration. Since the maximum dynamic stresses occur in regions subjected to low mean stresses, the part might stand high dynamic loadings regarding the Haigh's diagram. Then, the material damping can be considered as a helpful dissipation source. In the most cases the material damping is determined experimentally (see e.g. Figure 9-28). Also, the material modal damping ratio ξ_{int} can be determined as (Lazan, 1968)

$$17)\quad \xi_{\text{int}} = \frac{\int J\sigma_A^{\eta}\, dV}{4\pi\left(E_{p,B} + E_{p,C}\right)},$$

where J and η are material constants obtained from experiments, which for instance are equal to $J=2\times10^{-10}$ and $\eta=2.1$ at $500°C$ for X20Cr13 blade alloy. In equation (17) V indicates volume of the vibrating structure, $E_{p,B}$ and $E_{p,C}$ denote strain energies for the bending and centrifugal loading of the blade, respectively. These energies can be obtained from the static FE blade calculation. In terms of the dynamic stress σ_A in equation (17), the material damping is remarkable for martensitic steel alloys with *12%* chromium (Cr), and insignificant for most other steel alloys as it is presented in Figure 9-28. For instance for the X20Cr13 alloy, in ambient temperature the experimental material modal damping ratio ξ_{int} (Pfeiffer, 1985) changes linearly from 0.04% up to 0.27% by increasing the dynamic normal stress from *40 MPa* up to *100 MPa*. Below *30 MPa*, the material damping is usually not measured.

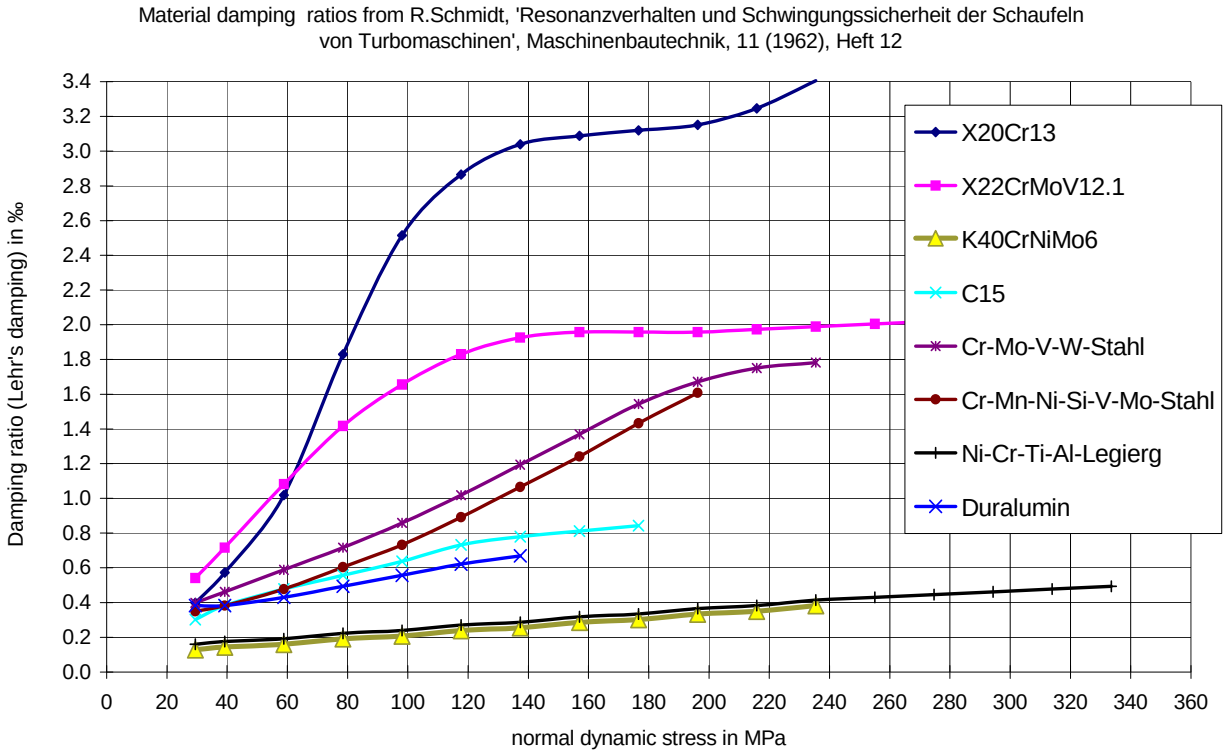

Figure 9-28: The modal damping ratio ξ_{int} in terms of the amplitude of the normal dynamic stress at the ambient temperature (Schmidt, 1962).

Besides the friction dissipation, the essential damping comes from the aero-dynamics under service conditions. The aero-damping can be determined either with the numerical flutter analysis (Lampert et al., 2004) or from the measured resonance frequency responses (Brown, 1981). Usually the aero-damping is evaluated experimentally from the measured resonance response function, since the blade is freestanding or then the contact forces acting on the airfoil interfaces are enough high, so that the friction dissipation can be neglected.

Not many experiments about the measured aero-damping properties are given in the open literature. For instance, Wolter (1980) measured dynamic stresses of *12* freestanding steam turbine blades, which were tested at the set-up with the real steam turbine shown in Figure 9-19. His measured resonance frequency response functions are presented in Figure 9-27a. Using the half-band method (Brown, 1981) the evaluated modal damping ratios varies between *0.21%* and *0.40%* for the partial arc admission excitation which corresponds to higher excitation loads (compare *P* and *A* in Figure 9-19c). For the nominal service condition, the damping ratios of these blades are slightly smaller and the damping ratios vary between *0.17%* and *0.19%* (Figure 9-29b). This is probably due to the lower contribution of the material damping to the reduction of resonance stresses in the blades. Considering uncertainties in this evaluation as well as in the measurements, the damping magnitudes of the analyzed freestanding steam turbine blades in service can alter between *0.2%* and *0.3%* mainly due to the aero-damping dissipation. In the comparable range between *0.23%* and *0.35%*, the experimental modal damping ratios ξ are found experimentally by Kielb and Abhari (2003) for the rotating high pressure blades.

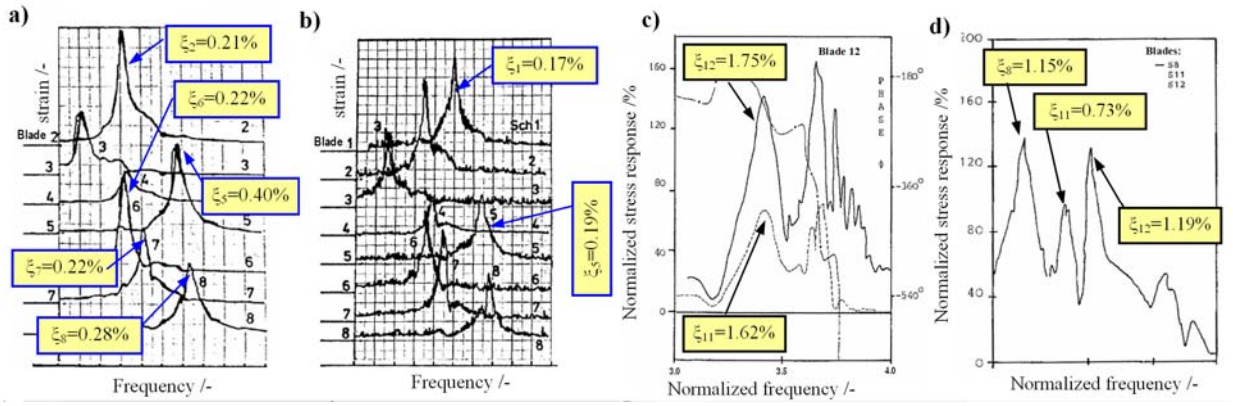

Figure 9-29: The experimental overall modal damping ratios where ξ_m denotes the damping value for blade *m* (Szwedowicz et al., 2008b).

a) Freestanding blades for excitation of the partial arc admission,

b) Freestanding blades under the nominal service condition with the ordinary stator arrangement

c) Blades with bolts for the excitation arranged by the partial arc admission

d) Blades with bolts under the nominal service condition with the ordinary stator arrangement

From Beckbissinger's (1982) experimental resonance response curves given in Figure 9-8c, the evaluated modal damping ratios of the blades (Figure 9-19) coupled by the bolts can vary between *1.6%* and *1.8%* for the excitation arranged by the partial arc admission. For the nominal service condition with the ordinary stator arrangement, which causes lower excitation, the damping values become smaller and alter between *0.7%* and *1.2%*. For all operation conditions, the evaluated overall damping magnitudes of the blades coupled by bolts are at least *3* times higher than those for the freestanding blades.

Besides the considered friction dissipation at the bolts, the friction damping can occur also in the root of the analyzed blade (Figure 9-19). For different centrifugal and bending loads, Matveev (1970) measured damping dissipation in the radial root with *2* fingers assembled by one pin to the rotor. For a centrifugal load of *30 kN* and a temperature of *350°C*, the measured damping ratio ξ at the analyzed root, made of titanium alloy, changes linearly from *0.03%* up to *0.70%* by increasing the bending airfoil load from zero to *350 N*. Recently, frictional capabilities at the blade roots like in dovetail or fir-tree joints are investigated more and more numerically (Charleux et al., 2004, Petrov, 2004).

Non-linear vibration simulations of the blade with friction dissipation can be done for the artificial viscous modal damping ratio to get reasonable resonance response level in the steady-state sweep analysis. This artificial viscous modal damping ratio should be corresponded to the expected aero-damping magnitude or to any reference values given in this report. Examples of the sweep steady-state dynamic analyses including friction dissipation are given in Figure 9-30.

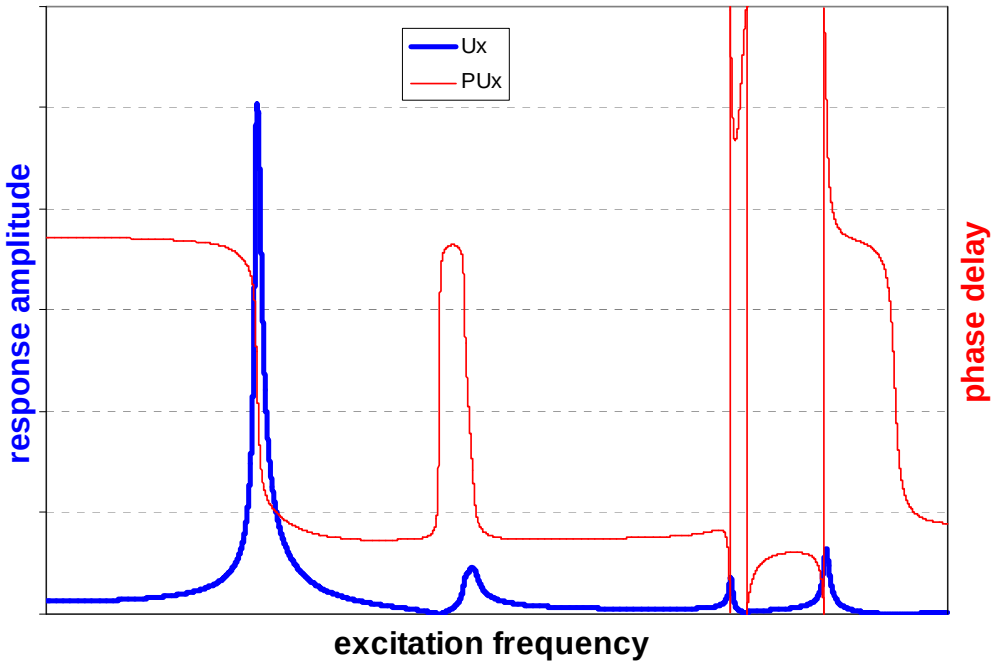

Figure 9-30: Numerical steady-state dynamic analyses including friction dissipation swept through the lowest resonance of the shrouded blade.

5.0 PERFORMANCE DIAGRAM OF VIBRATING BLADES

Usually the excitation acting on the rotating blades are not known very well, especially for the new design. Indeed, the static stresses are known quite good from the FE computation and the endurance ratios can be determined from the Haigh's diagram. These endurance ratios are treated then as the allowable resonance stresses in the design process. In addition, the dynamic blade analysis including friction dissipation must deal with physical uncertainties of the friction coefficient and contact stiffness. Another difficulty it is the evaluation of the damping magnitude from the resonance response function of the blade effectively damped by the friction dissipation. Then, the resonance response function has no more regular function shape as it can

be compared between *2* resonance frequencies of the out-of-phase and in-phase mode shapes of two blades damped with under-platform damper in Figure 9-31. For this case, the modal damping ratio ξ of the in-phase resonance frequency can be evaluated by using the half-band method as

$$18)\quad \xi = \frac{\omega_2 - \omega_1}{2\omega_r},$$

where the resonance frequency ω_r and frequencies ω_1, ω_2 are illustrated in Figure 9-32.

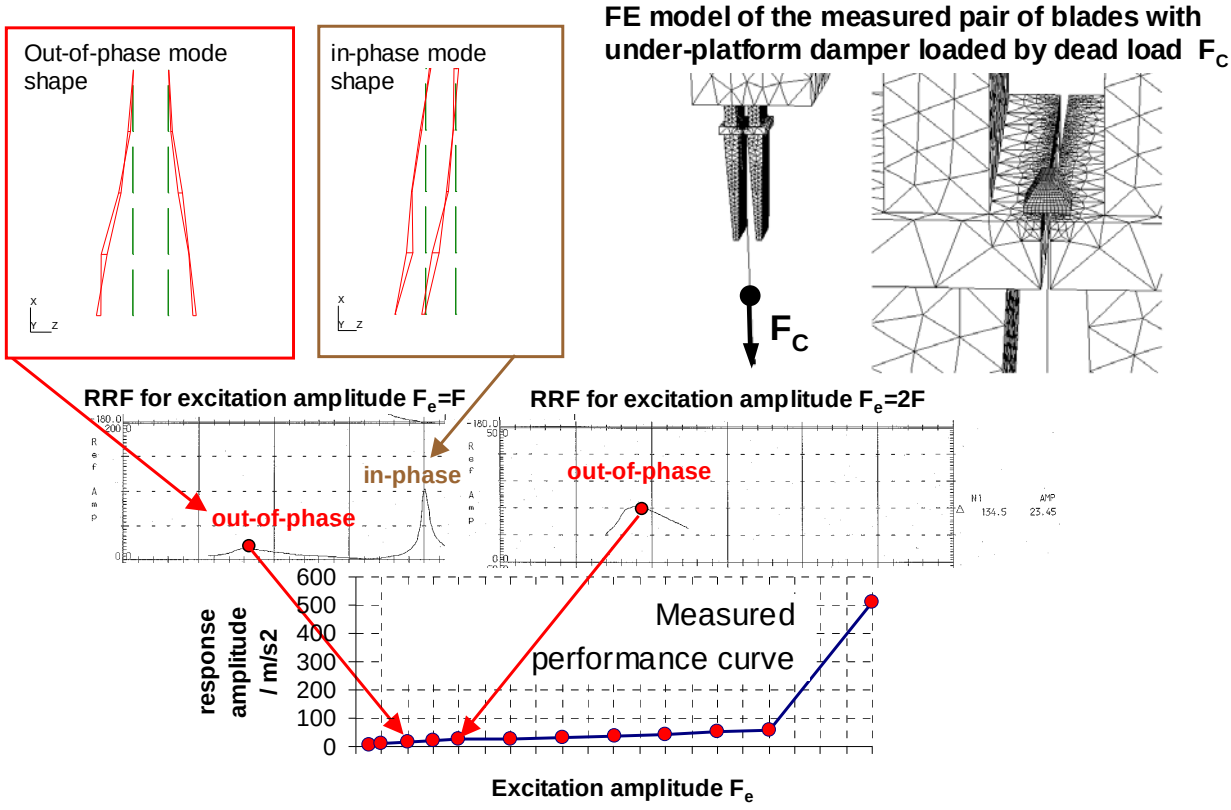

Figure 9-31: Creation of the experimental performance curves from the measured resonance response functions of the two blades with an under-platform damper tested at the non-rotating. set-up (Szwedowicz et al., 2001).

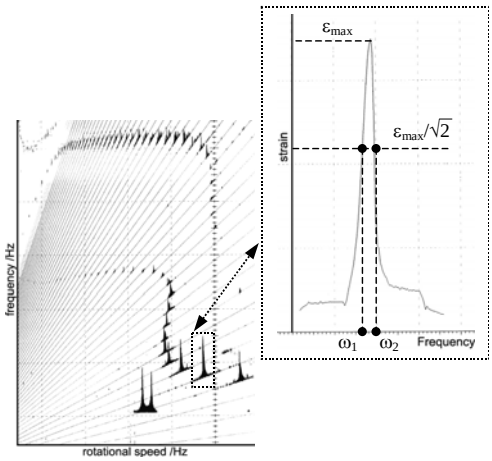

Figure 9-32: Application of the half-band method for the evaluation of the modal damping ratio ξ from the measured resonance response curve (RRF) of the shrouded disc (Szwedowicz et al., 2003).

The response of the out-of-phase resonance frequency in Figure 9-31 is suppressed so much that the half-band method cannot be applied considering the reliability of this evolution. Considering all these difficulties, Cameron et al. (1987) have introduced a very useful criterion for comparison of the vibrating blades with friction dissipation, which is called the performance diagram (Figure 9-31). As it is shown already in Figure 9-32, this evaluation concept merges all resonance stresses determined for different excitation amplitudes considering scatters in the physical data and relates them to the allowable resonance stress known from the Haigh's diagram.

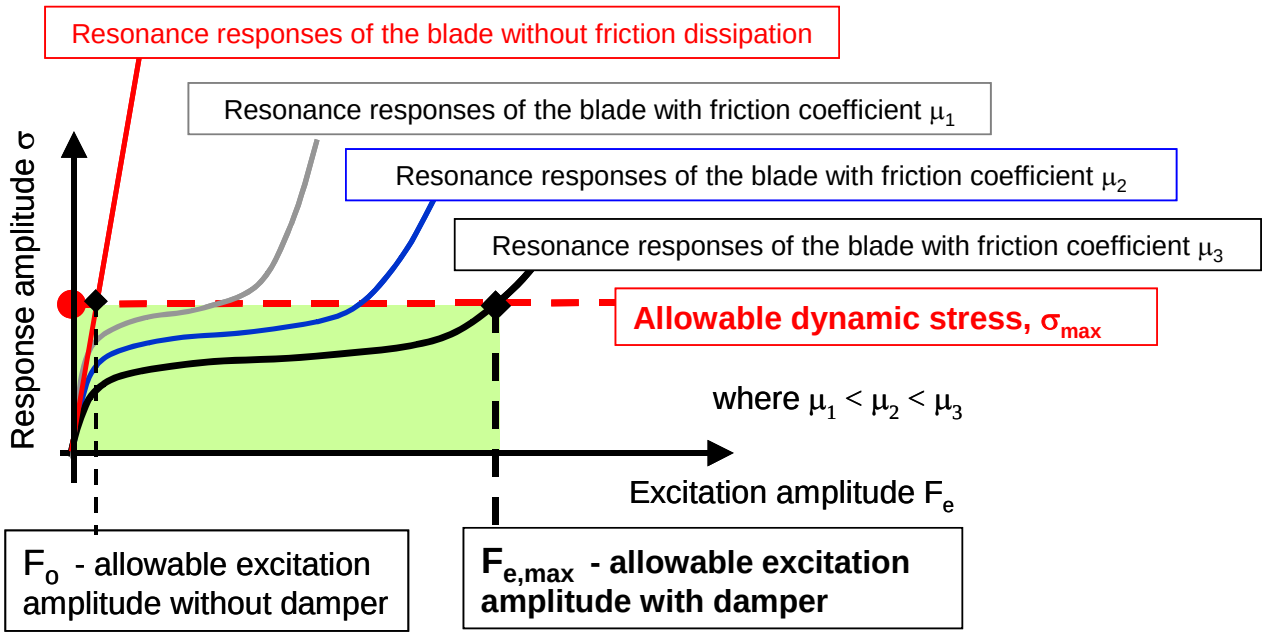

Figure 9-33: Explanation of the performance diagrams of blade vibrations with and without friction dissipation.

By increasing slip amplitudes of the damper on contact, a scatter in the measured blade responses increase too, what can be seen in the performance diagram in Figure 9-34. In the damper motion by increasing the excitation magnitude, like also on the shroud interface, three contact behaviors, such as:

- The sticking contact condition,
- The effective sliding of vibrating contacts,
- Chattering of sliding contacts

can be identified, as it is presented in Figure 9-34. For low excitations, the dynamic reactions on the contact are lower than the threshold friction force and then the blades are coupled with the friction damper (or on the shroud interface). Since the dynamic reactions exceed partially the friction threshold force on some regions of the contact area, the blade vibration is suppressed more by micro-slips on the damper (or on the shroud) interfaces. By further increase of excitation forces, larger regions of the contact area are in micro-slipping behavior and the blade damping steps up. The growth rate of the dynamic stresses is effectively smaller than that of the excitation increase. This contact behavior refers to the most effective damping performance. By further growing of the excitation forces acting on the blades, chattering of sliding contacts occurs, what corresponds to less effective frictional damping capabilities. This contact behavior is out of engineering interest. Usually the sticking and effective slipping contact behavior of the damper (or the shroud) is considered mainly in the design process.

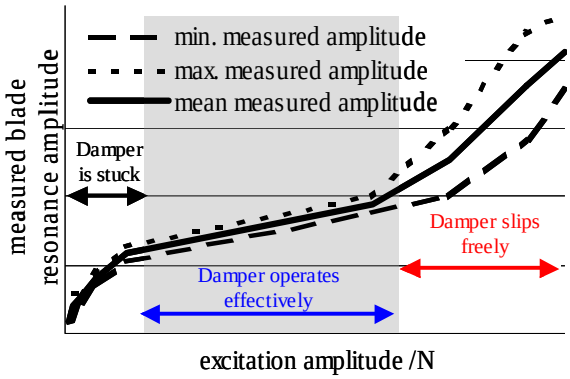

Figure 9-34: The measured performance diagram of the blade amplitudes damped by the under-platform damper (Figure 9-31), with the shown scatter in the experimental results increasing with bigger motions of the damper (Szwedowicz et al., 2001).

If the contact stiffness is determined properly, the numerical simulations of the blade vibration with friction damper can be predicted with very good agreements to the measured results. In Figure 9-35, the computed and measured performance diagrams of the blades with the under-platform damper are compared to each other with the satisfied agreement.

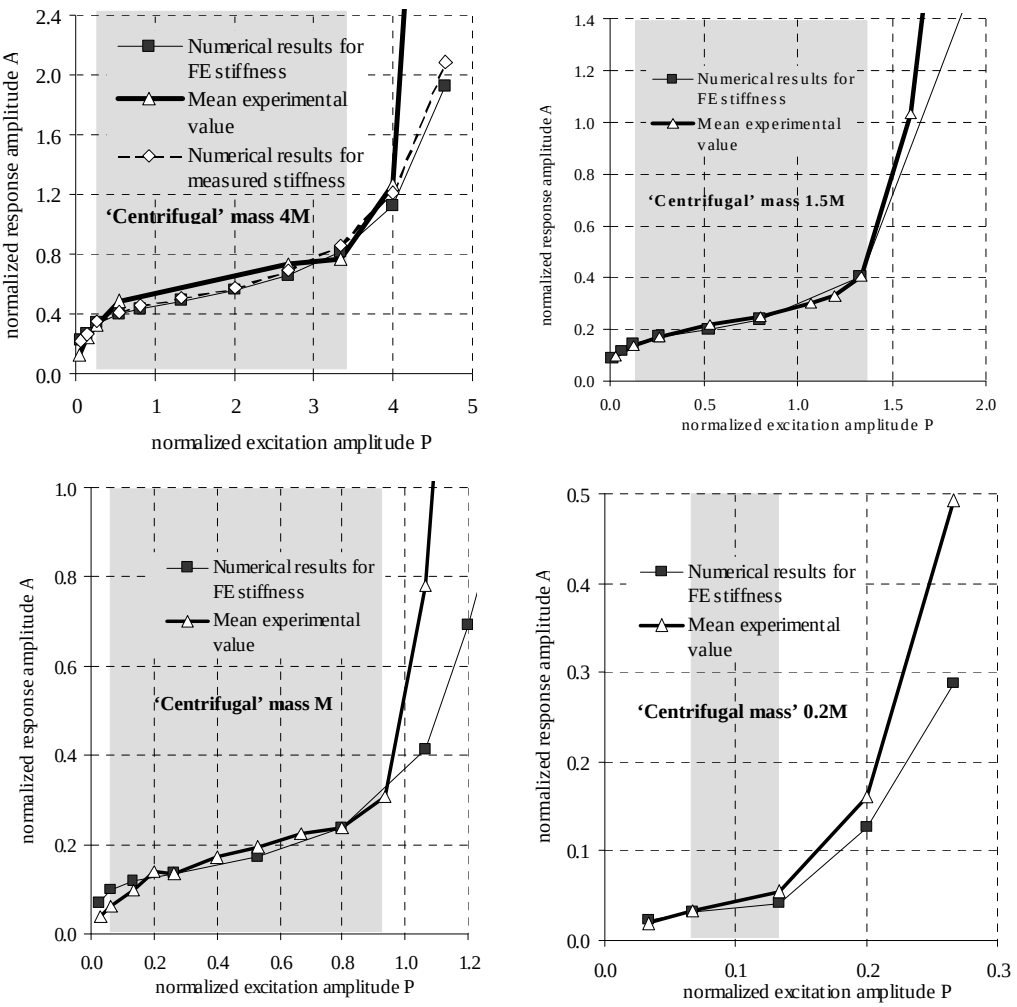

Figure 9-35: The measured and computed performance diagrams of two blades with the under-platform damper for different dead loads $F_C = M\,g$, where 'centrifugal' mass M denotes the mass hanging on the damper in the test and g is the gravity acceleration (see details in Szwedowicz et al., 2001).

In the development of friction dampers, the experimental validation of the computed damping performance is an important design stage. Frequently, the designed damper is tested firstly in the not-rotating set-up shown in Figure 9-31. At this set-up, the damper is loaded by the dead load $S = M\,g$, which corresponds to the expected centrifugal load F_C acting on the damper under the blade operation condition at the rotational speed Ω. The relationship between these forces is given by

$$19)\quad S = M\,g = m\,r\,(2\pi\Omega)^2,$$

where M is the mass hanging on the damper, $g=9.81\ m/s^2$ is acceleration of the gravity, r denotes the radial position of the damper in the bladed disc, m is the mass of the damper and Ω means the rotational speed of the turbine.

The next step in the damper design, it is the measurement of its damping performance in the rotating test rig. To save an effort of the experimental work, different dampers, for instance of various masses *m*, are arranged in different circumferential positions within the same bladed disc. Then, by measuring vibrations of these blades assembled with these various dampers, their damping capabilities can be proved experimentally during one measurement. This kind of the measurement is called a rainbow test. Also, the special test rigs can be found for pairs of two blades coupled with a damper. These blade pairs are placed diametrically on opposite disc sectors, as it is shown in Figure 9-9. The experimental and numerical performance results from this test rig at Ecole Centrale de Lyon in France of *2* real high pressure turbine blades damped with a thin-wall under-platform damper (Figure 9-9) are given in Figure 9-36.

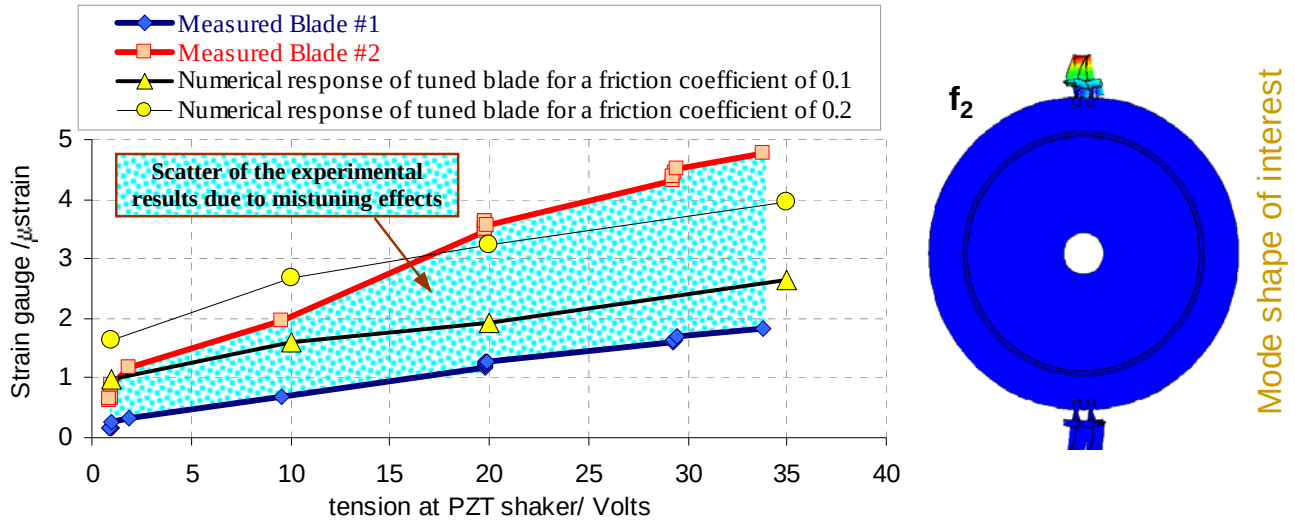

Figure 9-36: The experimental performance curves of the *2* mistuned rotating high pressure blades with the thin-walled damper (Figure 9-9) compared to the numerical ones of the tuned blades obtained for friction coefficients μ of *0.1* and *0.2* in vacuum (see details in Szwedowicz et al., 2006).

6.0 CONCLUSIONS

The design process of the rotating blades with friction damping capability can be done effectively by using a numerical tool based the harmonic balance method, which provides less time consuming solutions in relation to the FE time-marching approach. The reliable output of this process depends on few physical parameters, like the friction coefficient and the local contact stiffness. Although the utilization of the performance diagrams allows for moderating difficulties with a scatter nature of physical contact data, the designed friction damping mechanism needs to be proved experimentally. The whole process can require significant amount of time, budget and engineering efforts. Therefore, the already proved damping mechanism of the operating blading system can be scaled what was analyzed in Szwedowicz et al. (2008a and 2008b) and their final results are presented in Figures 9-37 and 9-38.

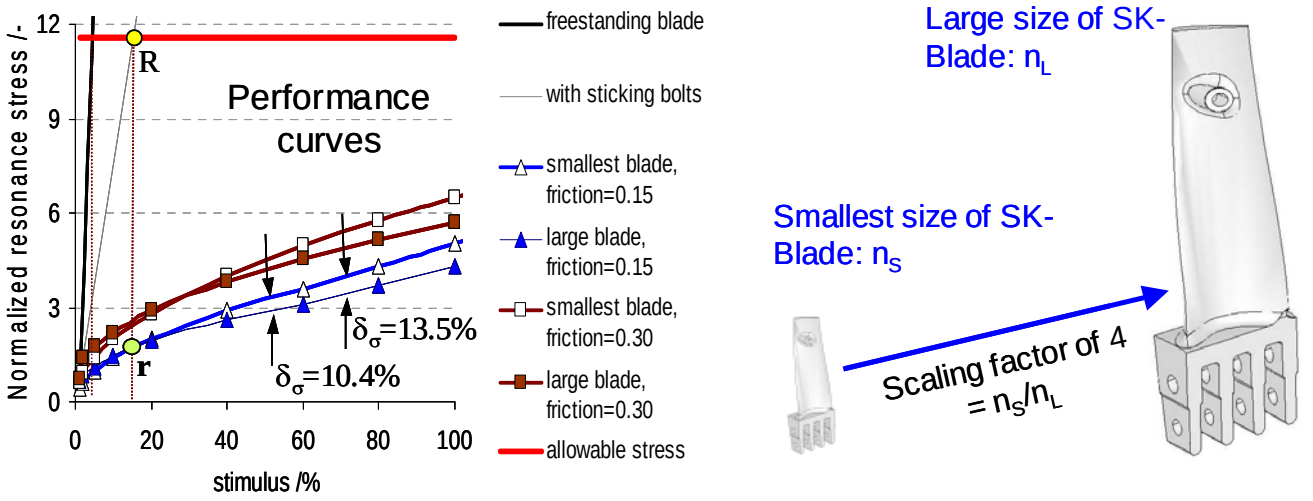

Figure 9-37: Performance curves of the smallest and large Siemens SK-blades with the friction bolts excited by the 8^{th} engine order at $\Omega_s=0.625\Omega_n$ under the service condition for the assumed aero-damping ξ_o of *0.5%*, where a stimulus of *100%* is equal to the static steam bending load at speed $\Omega_s=0.625\Omega_n$ (see details in Szwedowicz et al., 2008b).

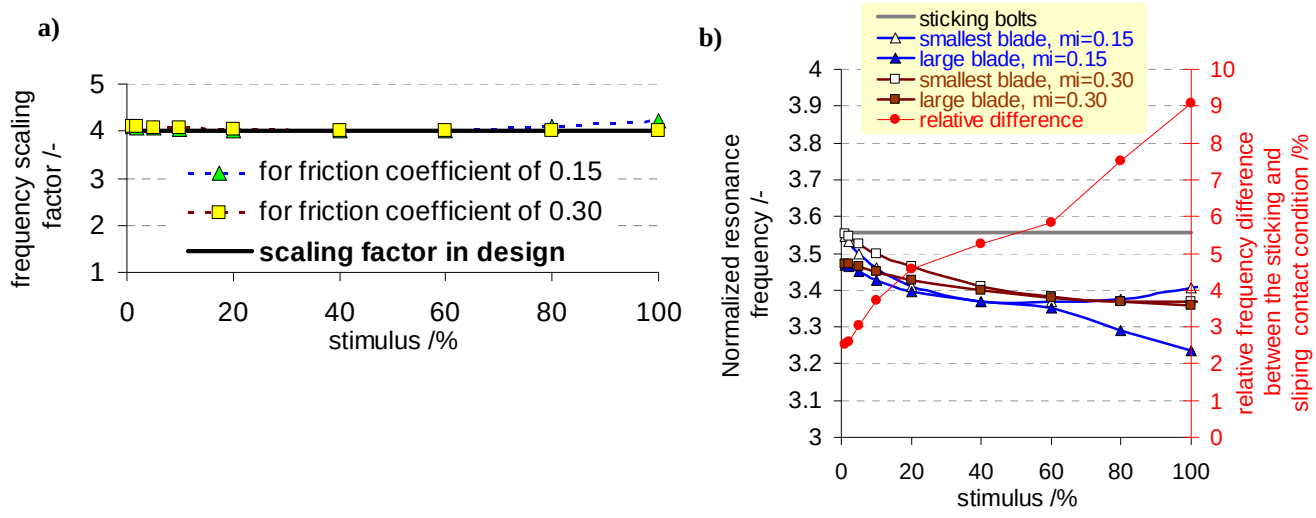

Figure 9-38: a) Validation of the scaling factors of the resonance frequencies $\upsilon_\omega=\omega_{small}/\omega_{large}$ determined from the non-linear dynamic simulations of the smallest and large Siemens SK-blade scaled by the design factor υ_O of *4* (Szwedowicz et al., 2008b), b) Sensitivity curves of the resonance frequencies of the smallest and large SK-blades excited by the 8th engine order at $\Omega_s=0.625\Omega_n$ under service conditions for the assumed aero-damping $\xi o=0.5\%$ (Szwedowicz et al., 2008b).

Regarding the scaling criteria, the computed dynamic stresses of both smallest and large blades, shown in Figure 9-37, should be identical to each other. For the considered friction coefficients of *0.15* and *0.30*, the computed resonance stresses of both blades differ from each other between *3.5%* and *14.3%* (see δ_σ in Figure 9-37). This is an acceptable result for the existing slight differences in the bolt dimensions applied to the smallest and large blades as it is described in Szwedowicz et al. (2008a and 2008b).

Both smallest and large Siemens SK-blades are principally identical on a *4* scale-up basis υ_O. For different stimuli, the scaling factors of their resonance frequencies obtained from the non-linear dynamic simulations are determined and shown in Figure 9-38a. All determined scale factors $\upsilon_\omega = \omega_{small}/\omega_{large}$ vary between *3.98* and *4.2*, and they are completely acceptable from the design point of view.

For getting predictable operation conditions of the bladed disc with the dampers, the friction dissipation on the damper should not change too much the blade frequency in relation to the sticking contact condition. For the analyzed Siemens SK-blades (Figure 9-37), in the whole considered stimulus range, the computed resonance frequencies of the smallest and large SK-blades differ maximally about *9%* with respect to their resonance frequencies for the contact with the stuck bolts as it is shown in Figure 9-38b.

The non-linear dynamic analyses provide obvious evidence of frictional dissipation for both smallest and large SK-discs in relation to the calculated resonance stresses with sticking bolts. The damping efficiency of the developed friction bolts for the vibrating blade is demonstrated in Figure 9-10. The resonance stress of the blade with stuck bolts can be reduced *6* times, if the friction dissipation takes place on the bolts. The numerical results presented in the performance curves and sensitivity frequency diagrams confirm the scalability of the damping capabilities between the smallest and large SK-blades for different stimuli, friction coefficients and aero-damping ratios. The field experiences with the different SK-blades, which operate with variable speed and in a variety of loading regimes, do not show any wear problems on the bolt and airfoil coatless contacts.

The here proposed non-linear numerical process could be applied to different types of blade couplings, like shrouds, winglets, lacing wires, zigzag pins or under-platform dampers. It has to be reminded finally, that the designed friction damping mechanism controls most effectively one resonance frequency of the rotating blades. Other resonance frequencies of the blade are damped less efficiently because of the changed rotational speed and excitation level. Therefore, in modern disc assemblies, the friction damping is optimized at the shroud interface by simultaneous application of the under-platform dampers (Petrov, 2007). This kind of the blade design allows for damping more resonances of the operating blade. Another option could be to develop the friction damper, whose damping performance is not so sensitive on the normal contact force. Two engineering attempts of this consideration are shown in Figure 9-39.

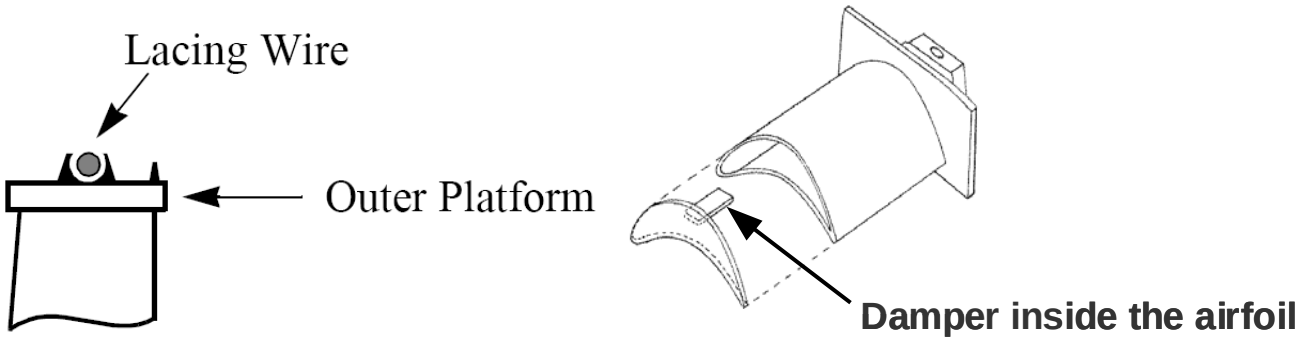

Figure 9-39: a) Lacing wire rolled within the shroud, which is used in one industrial steam turbine (Csaba, 1998a), b) Damper attached to the inner contour of the wall of the blade (Jones et al., 1975).

7.0 REFERENCES

Balmer, B., 1992, "Erhöhung der Dämpfung von Turbinenschaufeln durch Reibelement (Damping increase of turbine blades through friction damper)", FFV Report, No.436 and No.496, Heft 512, Frankfurt, Germany (in German)

Beckbissinger, L., 1982, „Schwingungsuntersuchungen von gekoppelten Turbinenlaufschaufeln bei verschiedenen Betriebszuständen", MSc Thesis Nr. D-54-82, Inst. für Thermische Strömungsmaschinen, Unv. Stuttgart

Burdekin, M., Back., N. and Cowley, A., 1978, "An elastic mechanism for micro-sliding characteristics between contacting machined surfaces", Journal Mech. Eng., Sci., **20(3)**, pp. 121-127

Borishanskii, K., 1974, "Characteristics of the Vibrations of Blades with Bandage Shelves" (in Russian), Problemy Prochnosti, No. 9, pp 97-102, September

Brown, W.G., 1981, "Determination of Damping Values for Turbine Blades", ASME Paper 81-DET-131, Proc. of the Design Engineering Technical Conference, Hartford, Connecticut, Sept. 20-23

Cameron, T.M., Griffin, J.H., Kielb, R.E. and Hossac, T.M., 1987, "An integrated approach for friction damper design", ASME booklet DE-Vol. 5, The role of damping in vibration and noise control, pp. 205-211

Cigeroglu, E., An, N. and Menq, C.-H., 2007, "Wedge damper modelling and forced response prediction of frictionally constrained blades", ASME Paper 2007-27963, Proceedings of ASME Turbo Expo 2007, May 14-17, Montreal, Canada

Charleux, D., Thouverez, F. and Lombard, J. P., 2004, "Three-dimensional Multi-harmonic Analysis of Contact and Friction in Dovetail Joints", Paper 348, Proceedings of the 22nd International Modal Analysis Conference, Dearborn, Michigan, USA, January

Csaba, G, 1998a, "Modelling Microslip Friction Damping and its Influence on Turbine Blade Vibrations", Master Thesis No. 519, Linköping University, Linköping, Sweden

Csaba, G., 1998b, "Forced Response Analysis in Time and Frequency Domains of a Tuned Bladed Disk With Friction Dampers", Transactions of the ASME, Journal of Sound and Vibration, Vol. **214**(3), pp. 395-412

Csaba, G., 1999, "Modelling of a micro-slip friction damper subjected to translation and rotation", ASME Paper 99-GT-149

Den Hartog, J. P., 1931, "Forced Vibrations with Combined Coulomb and Viscous Friction", Transactions of the ASME, Journal of Applied Mechanics **53**, APM-107, pp. 107-111

Den Hartog, J. P., 1956, "Mechanical Vibrations", the 4th Edition, McGraw-Hill Book Co., New York

Deresiewicz, H., December, 1957, "Oblique Contact of Nonspherical Elastic Bodies", Transactions of the ASME, Journal of Applied, **24**, pp. 623-624

DiCristofor, P. E. and Elledge, M., 2004, "Stress Redistribution for Increased Creep Life in the GE MS6001 B Second-Stage Blade", Transactions of the ASME, Journal of Engineering for Gas Turbines and Power, Vol. 126, January, pp. 127-130

Duffy, K. P., Bagley, R. L. and Mehmed, O., 2000, "On a Self-Tuning Impact Vibration Damper for Rotating Turbomachinery", Paper AIAA-2000-3100 (the American Institute of Aeronautics and Astronautics), Proceedings of the Joint Propulsion Conference, Huntsville, Alabama, July 17-19

Earles S.W.E., 1966, "Theoretical estimation of the frictional energy dissipation in a simple lap joint", Journal of Mechanical Engineering Science **8**, pp. 207-214

Earles S.W.E. and Mott, N., 1972, "A response prediction and optimization of a frictionally damped structure", Proceedings of the 13th International Machine Toll Design and Research Conference, September

Earles S.W.E. and Williams, E.J., 1972, "A Linearized Analysis for Frictionally Damped Systems", Journal of Sound and Vibration, Vol. **24** (4), pp. 445-458

Ewins, D.J., 1973, "Vibration Characteristics of Bladed Disc Assemblies", Journal Mechanical Engineering Science, Vol. 15, No. 3, pp 165-186

Figurski, H., 1981, "Schwingungsuntersuchung an einem realen Endstufenschaufelpaket mit eingelegten Dämpferelementen", Studienarbeit, Inst. für Thermische Strömungsmaschinen, Unv. Stuttgart

Figurski, H., 1982, „Schwingungsuntersuchungen von gekoppelten Turbinenlauf-Schaufeln bei verschiedenen Betriebszuständen", MSc Thesis, Inst. für Thermische Strömungsmaschinen, Unv. Stuttgart

Goetting, F, 2001, "Messung des Schwingungsverhaltens von verstimmten Beschaufelungen mit Reibelementen", Heft R 514, Proceedings of Informationstagung Turbinen, pp. 87-116, Dresden-Radebeul, September 27

Goetting, F., Sextro, W., Panning, L. and Popp, K., 2004, "Systematic Mistuning of Bladed Disk Assemblies with Friction Contacts", ASME Paper GT2004-53310, Proceedings of ASME Turbo Expo 2004, June 14-17, Vienna, Austria

Griffin, J. H., 1980, „Friction Damping of Resonant Stresses in Gas Turbine Engine Airfoils", Trans. of the ASME, Journal of Engineering for Power, Vol. 102, pp. 329-333

Griffin, J.H. and Labelle, R.F., 1996, "A Rational Method for Optimizing Shrouded Damping", ASME Paper 96-GT-402

Griffin, J. H. and Menq, C.-H., 1991, "Friction Damping of Circular Motion and Its Application to Vibration Control", Transactions of the ASME, Journal of Vibration and Acoustics, Vol. 113, pp. 225-229

Hertz, H., 1882, "On the Contact of Elastic Solids", Journal für die reine und angewandte Mathematik, Vol. 92, 156-171 (in German)

Jones, D.I.G., Nashif, A.D. and Stargardter, H., 1975, „Vibrating Beam Dampers for Reducing Vibrations in Gas Turbine Blades", Transactions of the ASME, Journal of Engineering for Power, pp. 111-116, January

Kelley, C. T., 2003, "Solving Nonlinear Equations with Newton's Method, No 1 in Fundamentals of Algorithms", SIAM, 2003. ISBN 0-89871-546-6

Kielb, J.J. and Abhari, R.S., 2003, "Experimental Study of Aerodynamic and Structural Damping in a Full-Scale Rotating Turbine", Trans. of the ASME, J. of Eng. for Gas Turbines and Power, Vol. 125, pp.102-112, January

Koh, K-H., Griffin, J.H., Filipp S. and Akay, A., 2004, "Characterization of Turbine Blade Friction Dampers", ASME Paper GT2004-53278, Proceedings of ASME Turbo Expo 2004, June 14-17, Vienna, Austria

Kielb, J.J. and Abhari, R.S., 2003, "Experimental Study of Aerodynamic and Structural Damping in a Full-Scale Rotating Turbine", Transactions of the ASME, Journal of Engineering for Gas Turbines and Power, Vol. 125, pp. 102-112

Lazan, B.J., 1968, "Damping Materials and Members in Structural Mechanics", Pregammon Press, New York

Lampert, P., Szymaniak, M. and Rzadkowski, R., 2004, "Unsteady Load of Partial Admission Control Stage Rotor of a Large Power Steam Turbine", ASME Paper GT2004-53886, Int. Gas Turbine & Aeroeng. Congress & Exh., June 14-117, Vienna, Austria

Matveev, V.V, Chaikoskii, B.S. and Rzhavin, L. N., 1970, "Damping capacity of the hinged locking joint of turbomachine compressor blades (in Russian)", Problemy Prochnosti, No. 12, pp. 106-109, December

Mott, N., 1970, "The optimum frictional damping for a vibrating structure", Thesis, University of London

Muszynska, A. and Jones, D.I.G., 1978, "On Discrete Modelization of Response of Blades with Slip and Hysteretic Damping", Proceedings of the 5th World Congress on Theory of Machines and Mechanisms, Montreal, Canada

Muszynska, A. and Jones, D.I.G., 1983, "On Tuned Bladed Disk Dynamics: Some Aspects of Friction Related Mistuning", Journal of Sound and Vibration, Vol. 86, No.1, pp. 107-128

Pfeiffer, R., 1985, „Einfluss unterschiedlicher Paketier-ungen auf Schwingungs-verhalten und Verbundfaktoren von Dampfturbinen-Beschaufelungen", PhD Thesis, Inst. für Thermische Strömungsmaschinen, Unv. Stuttgart

Panning L., Popp, K., Sextro., W, Goetting, F., Kayser, A. and Wolter, I., 2004, "Asymmetrical underplatform dampers in gas turbine bladings: Theory and Application", ASME Paper GT2004-53316, Proc. of ASME Turbo Expo, June 14-17, Vienna, Austria

Panning, L., 2005, "Auslegung von Reibelementen zur Schwingungsdämpfung von Turbienenschaufeln", PhD Thesis, Fortschritt-Berichte VDI, Reihe 11, Nr. 328, Institut fuer Dynamik und Schwingungen, Universität Hannover, Germany

Petrov, E.P. and Ewins, D.J., 2003, "Analytical Formulation of Friction Interface Elements for Analysis of Nonlinear Multi-harmonic Vibrations of Bladed Discs", ASME J. of Turbomachinery, Vol. 125, April, pp. 364-371

Petrov, E. P. and Ewins, D. J., 2004, "Analysis of Essentially Non-linear Vibration of Large-Scale Models For Bladed Discs With Variable Contact and Friction at Root Joints", Proceedings of the 8th International Conference on Vibrations in Rotating Machinery, Swansea, UK, September, pp. 163-172

Petrov, E.P., 2005, “Sensitivity Analysis of Nonlinear Forced Response for Bladed Discs with Friction Contact Interfaces”, ASME Paper GT2005-68935, Proceedings of ASME Turbo Expo 2005, June 6-9, Reno-Tahoe, Nevada, USA

Petrov, E.P., 2006, “Direct parametric analysis of resonance regimes for nonlinear vibrations of bladed discs”, ASME Paper GT2006-90147, Proceedings of the ASME Turbo Expo 2006, May 8-11, Barcelona, Spain

Petrov, E. P., 2007, “Explicit finite element models of friction dampers in forced response analysis of bladed disc”, ASME Paper 2007-27980, Proceedings of ASME Turbo Expo 2007, May 14-17, Montreal, Canada

Pfeiffer, R., 1985, „Einfluss unterschiedlicher Paketierungen auf Schwingungsverhalten und Verbundfaktoren von Dampfturbinen-Beschaufelungen”, PhD Thesis, Inst. für Thermische Strömungsmaschinen, Unv. Stuttgart

Rogers, P. F. and Boothroyd, G., 1975, “Damping at Metallic Interfaces Subjected to Oscillating Tangential Loads”, Transactions of the ASME, Journal of Engineering for Industry, pp. 1087 - 1093

Sanliturk, K. Y. and Ewins, D. J., 1996, “Modelling Two/Dimensional Friction Contact and Its Application Using Harmonic Balance Method”, ASME Journal of Sound and Vibration, Vol. 193(2), pp. 511-523

Sanliturk, K. Y., Imregun, M. and Ewins, D. J., 1999, “Harmonic Balance Vibration Analysis of Turbine Blades With Friction Dampers”, Transactions of the ASME, Journal of Vibration and Acoustics, Vol. 119, pp. 96 – 103, January

Sanliturk, K.Y., Ewins, D.J. and Stanbridge, A.B., 2001, “Under-platform Dampers for Turbine Blades: Theoretical Modelling, Analysis and Comparison with Experimental Data”, ASME J. Eng. for Gas Turbines and Power, Vol. 123, pp. 919-929, October

Scalzo, A.J., 1992, „High-Cycle Fatigue Design Evolution and Experience of Free-Standing Combustion Turbine Blades”, Transactions of the ASME, Journal of Engineering for Gas Turbines and Power, Vol. 114, pp. 284-292, April

Schmid, R., 1962, “Resonanzverhalten und Schwingungssicherheit der Schaufeln von Turbomaschinen”, Maschinenbautechnik, 11, Heft 12

Srinivasan, A.V., 1997, “Flutter and Resonant Vibration Characteristics of Engine Blades”, ASME Paper 97-GT-533, June 2-5, Orlando

Sever, I. A., Petrov, E., E. and Ewins, D., J., 2007, “Experimental and Numerical Investigation of Rotating Bladed Disk Forced Response Using Under-Platform Friction Dampers”, ASME Paper GT2007-27307, Proceedings of the ASME Turbo Expo, Montreal, Canada, May 14-17

Sextro, W. and Popp, K., 1996, “Dynamical Behaviour of a Bladed Disk with Friction Damper”, Proceedings of the 2nd European Nonlinear Oscillations Conference, Vol. 1, ISBN 80-85918-20-X, pp. 391-394

Sextro, W. Popp, K. and Wolter, I., 1997, “Improved Reliability of Bladed Disks to Friction Dampers”, ASME Paper 97-GT-189, Proceedings of ASME Tubro Expo 1997, Orlando, USA

Sextro, W., 2000, “The Calculation of the Forced Response of Shrouded Blades with Friction Contacts and Its Experimental Verification”, ASME Paper 2000-GT-540, Proceedings of the ASME Turbo Expo 2000, Munchen, Germany

Sextro, W., 2002, “Dynamical Contact Problems with Friction - Models, Methods, Experiments and Applications”, Habilitationsschrift, Lecture Notes in Applied Mechanics, Vol. 3, Springer-Verlag, Heidelberg

Siewert, C., Panning, L., Schmidt-Fellner, A. and Kayser, A., 2006, „The Estimation of the Contact Stiffness for Directly and Indirectly Coupled Turbine Blading”, ASME Paper GT2006-90473, The proceedings of the ASME Turbo Expo, May 8-11, Barcelona, Spain

Swikert, M.A. and Johnson, R.L., 1968, “Friction and Wear under Fretting Conditions of Materials for Use As Wire Friction Dampers of Compressor Blade Vibration”, NASA Technical Note TN D-4630, Washington, July

Szwedowicz, J., Kissel, M., Ravindra, B. and Keller, R., 2001, „Estimation of Contact Stiffness and its Role in the Design of a Friction Damper”, Proceedings of ASME Turbo Expo, 2001-GT-0290

Szwedowicz, J., Visser, R., Sextro, W. and Masserey, P.A., 2003, “On Forced Vibrations of Shrouded Turbine Blades”, ASME Paper GT2003-38808, Proc. of ASME Turbo Expo 2003, June, Atlanta, USA, pp. 1-13, New Orleans, USA

Szwedowicz, J., Slowik, S., Mahler, A. and Hulme, C.J., 2005, “Nonlinear Dynamic Analyses of a Gas Turbine Blade For Attainment of Reliable Shroud Coupling”, ASME Paper No. GT2005-69062, Proceedings of ASME Turbo Expo 2005, June 06-09, Reno-Tahoe, USA

Szwedowicz, J., Gibert, C., Sommer, T.P. and Kellerer, R., 2006b, “Numerical and Experimental Damping Assessment of a Thin-Walled Friction Dampers in the Rotating Set-up with High Pressure Turbine Blades”, ASME Paper GT2006-90951, Proceedings of the ASME Turbo Expo, May 8-11, Barcelona, Spain

Szwedowicz, J., Secall-Wimmel, T., Dünck-Kerst, P., Sonnenschein, A., Regnery, D. and Westfahl, M., 2008a, “Scaling Concept for Axial Turbine Stages with Loosely Assembled Friction Bolts: The Linear Dynamic Assessment”, Transactions of the ASME, Journal of Engineering for Gas Turbines and Power, Vol. 130, No. 032504, pp. 1 – 12, May

Szwedowicz, J., Secall-Wimmel, T. and Dünck-Kerst, P., 2008b, “Damping Performance of Axial Turbine Stages With Loosely Assembled Friction Bolts: The Nonlinear Dynamic Assessment”, Transactions of the ASME, Journal of Engineering for Gas Turbines and Power, Vol. 130, No. 032505, pp. 1 – 14, May

Szwedowicz, J., Sextro, W., Visser, R. and Masserey, A.P., 2008c, “On Non-Linear Forced Vibration of Shrouded Turbine Blades”, Transactions of the ASME, Journal of Turbomachinery, Vol. **130**, No. 1, pp. 011002-1 / 011002-9, ISSN 0889-504X, January

Treyde, T., 1994, „Koppeldaempfungen und –steifigkeiten zwischen den Kontakflaechen der Deckplatten von Laufschaufeln (Contact damping and stiffness between the interfaces of the shrouds of rotating turbine blades)”, FVV Report No. 525, BMWi / AIF-No. 8803, Frankfurt

Vingsbo, O. and Söderberg, D, 1988, „On Fretting Maps”, Wear, Vol. 126, pp. 131-147

Wachter, J., Pfeiffer, R. and Jarosch, J., 1983, „Experimental Study To Gain Insight in the Vibration Characteristics of a Steam Turbine LP-Wheel With Lashing Pins", ASME Proc. "Vibration of Bladed Disk Assemblies" Nr. 83-72174, Dearborn, Michigan, Sept. 11-14, pp. 83-89

Wand J.H. and Chen, W. K., 1992, "Investigation of the Vibration of a Blade with Friction Damper by HBM", ASME Paper 92-GT-8, Proceedings of the International Gas Turbine and Aeroengine Congress and Exposition, Cologne, Germany, June 1-4

Wang, J.H. and Yau, H.Y., 1990a, "Design of Shroud Interface-Angle to Minimize the Forced Vibration of Blades", ASME Paper No. 90-GT-247

Wang, J.H. and Yau, H.Y., 1990b, "Design of Blade-Shroud to Minimize the Sensitivity of Response to Preload Mistuning", Proc. of the 3rd International Conf. on Rotordynamics, Sept. 9-12, Lyon, France

Wang, J.H. and Shieh, W.L., 1991, "The Influence of Variable Friction Coefficient on the Dynamic Behaviours of Blade with Friction Damper", J. of Sound and Vibration, Vol. 149, pp. 137-145

Wang, J.H. and Chen, W.K., 1993, "Investigation of a Blade with a Friction Damper by HBM", ASME Transaction, J. of Engineering for Gas Turbines and Power, Vol. 115, pp. 294-299

Williams, E.J. and Earles, S.W.E., 1974, „Optimization of the Response of Frictionally Damped Beam Type Structures with Reference to Gas Turbine Compressor Blading", Transactions of the ASME, Journal of Engineering for Industry, pp. 471-476, May

Wolter, I., 1980, „Experimentelle Untersuchung des Schwingungsverhaltens von Turbinenlaufschaufeln unter realen Betriebsbedingungen mit und ohne Kopplung durch einen eingelegten Dämpferdraht", PhD Thesis No. T81/128, Inst. für Thermische Strömungsmaschinen, University of Stuttgart

Yang, B.D. and Menq, C.-H., 1998a, "Characterization of Contact Kinematics and Application to the Design of Wedge Dampers in Turbomachinery Blading, Part I: Stick-slip Contact Kinematics", ASME J. of Eng. For Gas Turbines and Power, Vol. 120, No.2, pp.410-417

Yang, B.D. and Menq, C.-H., 1998b, "Characterization of Contact Kinematics and Application to the Design of Wedge Dampers in Turbomachinery Blading, Part II: Prediction of Forced Response and Experimental Verification", ASME J. of Eng. For Gas Turbines and Power, Vol. 120, No.2, pp.418-423

Zimitrowicz, A., 1981, "A Vibration Analysis of a Turbine Blade System Damped by Dry Friction Forces", International Journal of Mechanical Science, Vol. **23**(2), pp. 741-761